Phys. Med. Biol. **42** (1997) 1–39. Printed in the UK PII: S0031-9155(97)36090-4

REVIEW

X-ray detectors for digital radiography

M J Yaffe and J A Rowlands

Imaging Research Program, Sunnybrook Health Science Centre, The University of Toronto, 2075 Bayview Avenue, Toronto, Ontario, Canada M4N 3M5

Received 29 March 1996, in final form 16 August 1996

Abstract. Digital radiography offers the potential of improved image quality as well as providing opportunities for advances in medical image management, computer-aided diagnosis and teleradiology. Image quality is intimately linked to the precise and accurate acquisition of information from the x-ray beam transmitted by the patient, i.e. to the performance of the x-ray detector. Detectors for digital radiography must meet the needs of the specific radiological procedure where they will be used. Key parameters are spatial resolution, uniformity of response, contrast sensitivity, dynamic range, acquisition speed and frame rate. The underlying physical considerations defining the performance of x-ray detectors for radiography will be reviewed. Some of the more promising existing and experimental detector technologies which may be suitable for digital radiography will be considered. Devices that can be employed in full-area detectors and also those more appropriate for scanning x-ray systems will be discussed. These include various approaches based on phosphor x-ray converters, where light quanta are produced as an intermediate stage, as well as direct x-ray-to-charge conversion materials such as zinc cadmium telluride, amorphous selenium and crystalline silicon.

1. Introduction

The benefits of acquisition of medical radiological images in digital form quickly became obvious following the introduction of computed tomography (CT) by Hounsfield (1973). These benefits include greater precision of recording the information, increased flexibility of display characteristics and ease of transmitting images from one location to another over communications networks.

Computed tomography is a rather sophisticated application of digital radiography, and more recently, digital approaches to simpler, more mainstream imaging techniques such as angiography and conventional projection radiography as well as to ultrasound and nuclear medicine imaging have been developed. Part of the reason for this chronology was that CT was immediately accepted because of the obvious benefits of true transverse tomography and the ability of CT to display subtle differences in tissue attenuation. These outweighed the desire for high spatial resolution which could not be achieved with the coarse detectors and limited computer capacity available at the time, but which could be obtained with standard radiographic projection imaging.

The development of improved detector technologies, as well as much more powerful computers, high-resolution digital displays and laser output devices was necessary before digital radiography could progress further. Initially, it was thought that digital radiography would have to match the very demanding limiting spatial resolution performance of film-based imaging. However, film imaging is often limited by a lack of exposure latitude due to the film's characteristic curve and by noise associated with film granularity and inefficient use of the incident radiation. Further experience has suggested that a high value of limiting

0031-9155/97/010001+39$19.50

resolution is not as important as the ability to provide excellent image contrast over a wide latitude of x-ray exposures for all spatial frequencies up to a more modest limiting resolution (Yaffe 1994). A digital radiographic system can provide such performance, as well as allowing the implementation of computer image processing techniques, digital archiving and transmission of images and extraction of medically useful quantitative information from the images.

Historically, there has been a strong interest in developing digital imaging systems for chest radiography because of the inherent weaknesses of film-screen systems in providing adequate latitude and simultaneously good contrast over the lung and mediastinal regions and the desire to implement features such as image processing, teleradiology and digital archiving and retrieval systems (PACS). Tesic *et al* (1983) described a single-line-scanning digital system for chest radiography which used an array of 1024 discrete photodiodes coupled to a gadolinium oxysulphide phosphor. This required a scan time of 4.5 s and provided a limiting spatial resolution of 1 cycle/mm. Goodman *et al* (1988) and Fraser *et al* (1989) reviewed the strengths and weaknesses of various approaches to digital chest radiography available at that time. They identified the potential for digital chest radiography while indicating improvements that would be necessary for the technique to become accepted by radiologists.

Digital systems for subtraction angiography and for some types of projection radiography are now in widespread clinical use and specialized systems for demanding applications such as mammography are currently under development. The availability of such digital systems will potentially permit the introduction of computer-aided diagnosis (Chan *et al* 1987, Giger *et al* 1990). There have been several previous reviews of digital imaging detector technology, notably by Rougeot (1993).

2. Digital images

Virtually all x-ray images are based on transmission of quanta through the body, with contrast occurring due to variations in thickness and composition of the internal anatomy. The x-ray transmission pattern in the plane of the imaging system can be considered as a continuous variation of x-ray fluence with position. A hypothetical pattern is shown in one dimension in figure 1(*a*). An analogue imaging detector attempts to reproduce this pattern faithfully, for example as variations of optical density on a developed film emulsion. In principle, these variations are spatially continuous and, provided that enough x-ray quanta are used, they are also continuous on the intensity scale.

A schematic diagram of a generic digital radiography system is given in figure 2. Here, the analogue image receptor is replaced by a detector that converts energy in the transmitted x-ray beam into an electronic signal which is then digitized and recorded in computer memory. The image can then be processed, displayed, transmitted or archived using standard computer and digital communication methods.

In a digital imaging system, at some stage, the x-ray transmission pattern is sampled both in the spatial and intensity dimensions, as illustrated in figure 1(*b*). In the spatial dimension, samples are obtained as averages of the intensity over picture elements or *pixels*. These are generally square areas, which are spaced at equal intervals throughout the plane of the image. In the intensity dimension, the signal is binned into one of a finite number of levels. This is normally a power of 2 and the value, n, of this power is designated as the number of bits to which the image is digitized. Intensity values of the digital image can, therefore, only take on discrete values, and information regarding intermediate intensities and variations on a subpixel scale is lost in the digitization.

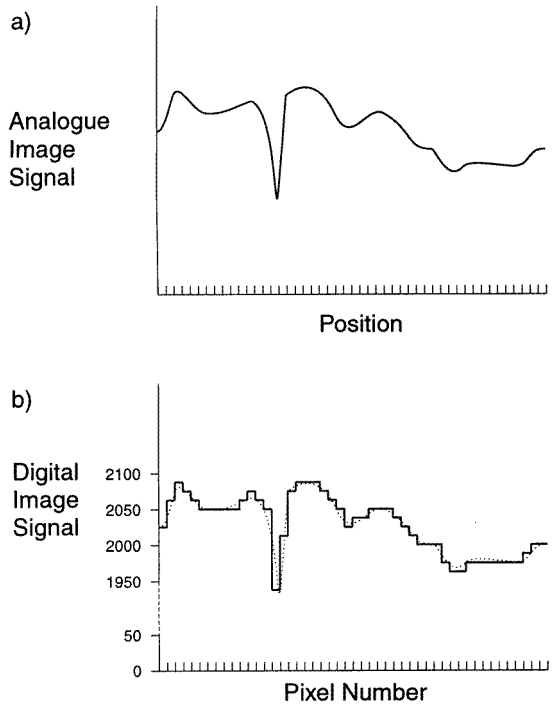

Figure 1. Concepts of digital imaging. (*a*) Profile of an analogue image varies continuously, both spatially and in signal intensity. (*b*) In a digital image, sampling takes place at discrete intervals in position and intensity.

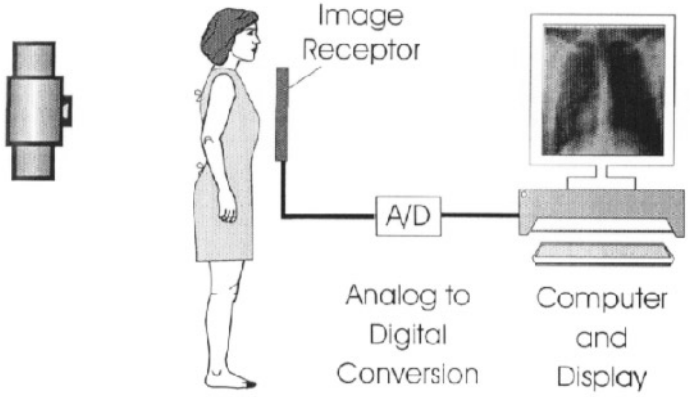

Figure 2. Schematic diagram of a digital radiography system.

To avoid degradation of image quality in the digitization process, it is important that the pixel size and the bit depth are appropriate for the requirements of the imaging task and are consistent with the intrinsic spatial resolution and precision of the image as determined by such fundamental limiting factors as the focal spot unsharpness, anatomical motion and the level of quantum noise.

3. Detector properties

Important detector properties are: field coverage, geometrical characteristics, quantum efficiency, sensitivity, spatial resolution, noise characteristics, dynamic range, uniformity, acquisition speed, frame rate and cost. In most, if not all, cases different detector technologies necessitate compromises among these factors.

3.1. Field coverage

The imaging system must be able to record the transmitted x-ray signal over the projected area of the anatomy under investigation. One can estimate the requirements of digital radiology detectors from the image receptors used for conventional imaging. For example, chest radiography requires an imaging field of 35 cm $\times$ 43 cm, while mammography can be accommodated by a receptor of dimensions 18 cm $\times$ 24 cm or 24 cm $\times$ 30 cm. Image intensifiers used for fluoroscopy and film photofluorography provide circular fields with diameters ranging from 15 cm to 40 cm. In addition, because of x-ray beam divergence, the image always undergoes some degree of radiographic magnification. Often, this is only on the order of 10%; however, for examinations where magnification is intentionally applied, this can be a factor of 2 or more and, therefore, the clinical use must be carefully considered when specifying detector size requirements.

3.2. Geometrical characteristics

Some of the factors to be considered here are the 'dead regions' that may exist within and around the edges of the detector. In an electronic detector used for digital radiography, these might be required for routing of wire leads or placement of auxiliary detector components such as buffers, clocks, etc. Dead regions can also result when a large-area detector is produced by abutting smaller detector units (tiling). For detectors composed of discrete sensing elements, we can define the fill-factor as the fraction of the area of each detector element that is sensitive to the incident x-rays. In some applications (for example mammography) it is important that the detector has negligible inactive area on one or more edges to avoid excluding tissue from the image. This may preclude the use of detectors with bulky housings, such as vacuum image intensifiers, from those applications. In any case, dead area within the detector results in inefficient use of the radiation transmitted by the patient unless prepatient collimation can be used to mask the radiation that would fall on these dead areas. Usually, because of alignment complexity and focal spot penumbra, this is not practical.

Another geometrical factor which must be considered is distortion. A high-quality imaging system will present a faithful spatial mapping of the input x-ray pattern to the image output. The image may be scaled spatially; however, the scaling factor should be constant over the image field. Distortion will cause this mapping to become nonlinear. It may become spatially or angularly dependent. This may be the case when lens, fibre or electron optics are used in the imaging system and give rise to 'pincushion' or 'barrel' distortion.

Finally, it should be noted that digital detectors can be of two general types, captive sensors or replaceable cassettes. In the former, the receptor and its readout are integrated into the x-ray machine. While this requires a specially designed machine with higher capital cost, it also eliminates the need for loading, unloading and carrying of cassettes to a separate reader and the labour costs involved. As well, the use of a single or a limited number of

receptors simplifies the task of correction for non-uniformities of the receptors (see below). A reusable cassette system may be advantageous where a high degree of portability or flexibility is required, such as in intensive care situations or operating theatres, and has the advantage of being compatible with existing radiographic units.

3.3. Quantum efficiency

The initial image acquisition operation is identical in all x-ray detectors. In order to produce a signal, the x-ray quanta must interact with the detector material. The probability of interaction or *quantum efficiency* for quanta of energy $E = h\nu$ is given by

$$\eta = 1 - \mathrm{e}^{-\mu(E)T} \tag{1}$$

where μ is the linear attenuation coefficient of the detector material and T is the active thickness of the detector. Because virtually all x-ray sources for radiography are polyenergetic, and, therefore, emit x-rays over a spectrum of energies, the quantum efficiency must either be specified at each energy or must be expressed as an 'effective' value over the spectrum of x-rays *incident on the detector*. This spectrum will be influenced by the filtering effect of the patient which is to 'harden' the beam, i.e. to make it more energetic and, hence, more penetrating.

The quantum efficiency can be increased by making the detector thicker or by using materials which have higher values of μ because of increased atomic number or density. The quantum efficiency versus x-ray energy for various thicknesses of some detector materials is plotted in figures 3 and 4. The quantum efficiency will in general be highest at low energies, gradually decreasing with increasing energy. If the material has an atomic absorption edge in the energy region of interest, then quantum efficiency increases dramatically above this energy, causing a local minimum in η for energies immediately below the absorption edge.

At diagnostic x-ray energies, the main interaction process is the photoelectric effect because of the relatively high atomic number of most detector materials. Interaction of an x-ray quantum with the detector generates a high-speed photoelectron. In its subsequent loss of kinetic energy in the detector, excitation and ionization occur, producing the secondary signal (optical quanta or electronic charge).

3.4. Spatial resolution

Spatial resolution in radiography is determined both by the detector characteristics and by factors unrelated to the receptor. The second category includes unsharpness arising from geometrical factors. Examples are: 'penumbra' due to the effective size of the x-ray source and the magnification between the anatomical structure of interest and the plane of the image receptor or relative motion between the x-ray source, patient and image receptor during the exposure. Detector-related factors arise from its effective aperture size, spatial sampling interval between measurements and any lateral signal spreading effects within the detector or readout.

Detectors for digital radiography are often composed of discrete elements, generally of constant size and spacing. The dimension of the *active* portion of each detector element defines an *aperture*. The aperture determines the spatial frequency response of the detector. For example, if the aperture is square with dimension, d, then the modulation transfer function (MTF) of the detector will be of the form sinc f, where f is the spatial frequency along the x or y directions, and the MTF will have its first zero at the frequency $f = d^{-1}$, expressed in the plane of the detector (figure 5). A detector with $d = 50$ μm will have an

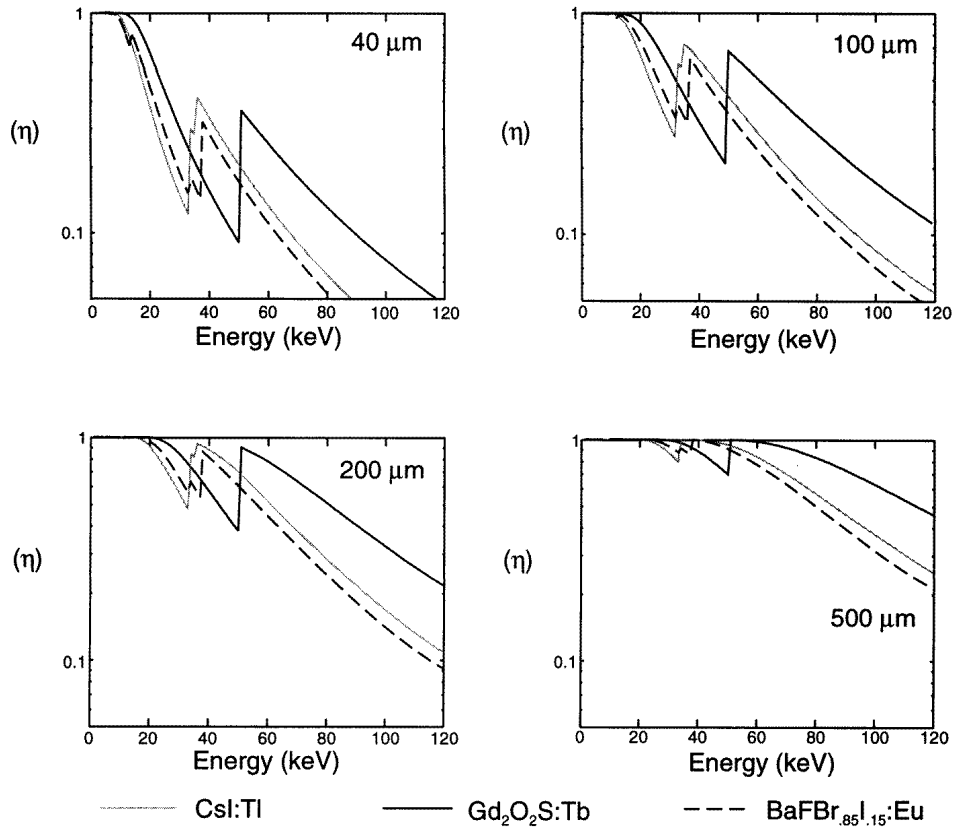

Figure 3. Quantum interaction efficiency, η, of various thicknesses of selected phosphors. Note that, except for CsI, the phosphor particles are combined with a binder, causing the packing density to be reduced (typically to 50%), so that the screen thickness must be increased to provide the attenuation values shown.

MTF with its first zero at $f = 20$ cycles/mm. Because of magnification, this frequency will be higher in a plane within the patient.

Also of considerable importance is the sampling interval, p, of the detector, i.e. the pitch in the detector plane between sensitive elements or measurements. The sampling theorem states that only spatial frequencies in the pattern below $(2p)^{-1}$ (the Nyquist frequency) can be faithfully imaged. If the pattern contains higher frequencies, then a phenomenon known as *aliasing* occurs wherein the frequency spectrum of the image pattern beyond the Nyquist frequency is mirrored or folded about that frequency in accordion fashion and added to the spectrum of lower frequencies, increasing the apparent spectral content of the image at these lower frequencies (Bendat and Piersol 1986). In a detector composed of discrete elements, the smallest sampling interval in a single image acquisition is $p = d$, so that the Nyquist frequency is $(2d)^{-1}$ while the aperture response falls to 0 at twice that frequency (higher if the dimension of the sensitive region of the detector element is smaller than d, for example because the fill-factor of the detector element is less than 1.0).

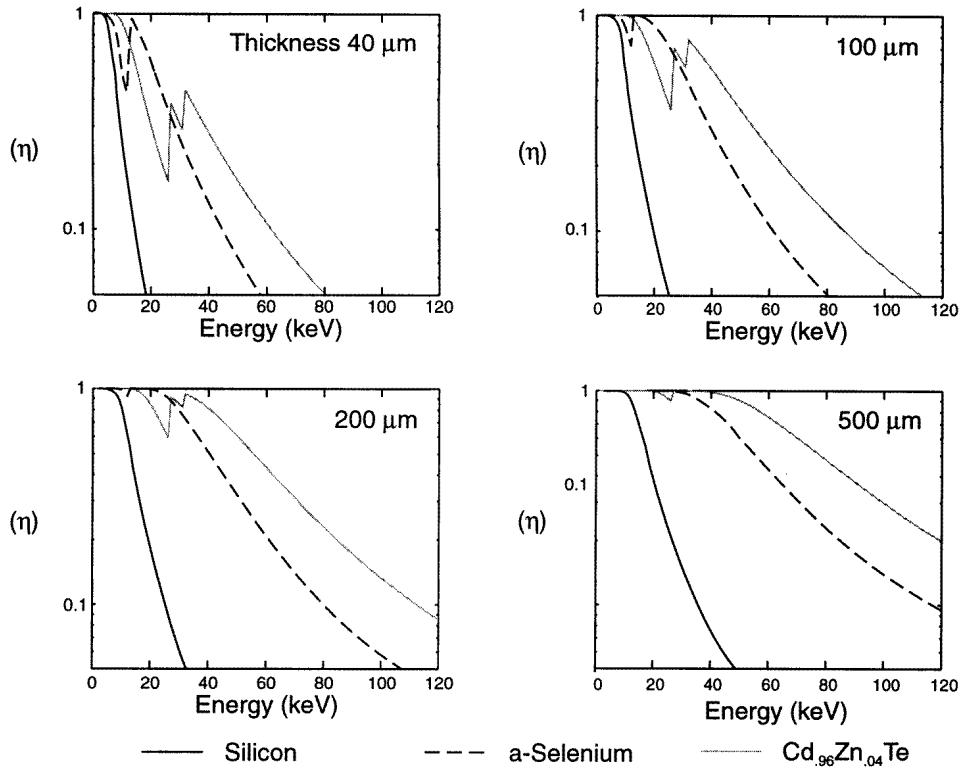

Figure 4. Quantum interaction efficiency, η, of selected direct conversion detector materials.

Aliasing can be avoided by 'band limiting' the image, i.e. attenuating the higher frequencies such that there is no appreciable image content beyond the Nyquist frequency. The blurring associated with the focal spot may serve this purpose. Note that this does not prevent the aliasing of high spatial frequency noise. Alternative methods which reduce aliasing effects of both signal and noise require the sampling frequency of the imaging system to be increased. One method for achieving this, known as *dithering*, involves multiple acquisitions with a physical motion of the detector by a fraction of the pixel pitch between successive acquisitions. The subimages are then combined to form the final image. This effectively reduces p, thereby providing a higher Nyquist frequency. Some detectors are not pixellated at the x-ray absorption stage, but rather d and p are defined in their readout mechanism. This is the case for the photostimulable phosphor detector system described below, where the phosphor plate is continuous, but the laser readout samples the plate at discrete locations. This can provide some flexibility in independently setting the sampling interval (scanning raster) and effective aperture size (laser spot size) to avoid aliasing. Issues of sampling in digital radiographic systems have been reviewed by Dobbins (1995).

In the overall design of an imaging system, it is important that other physical sources of unsharpness be considered when the aperture size and sampling interval are chosen. If, for example, the MTF is limited by unsharpness due to the focal spot, it would be of little value to attempt to improve the system by designing the receptor with smaller detector elements.

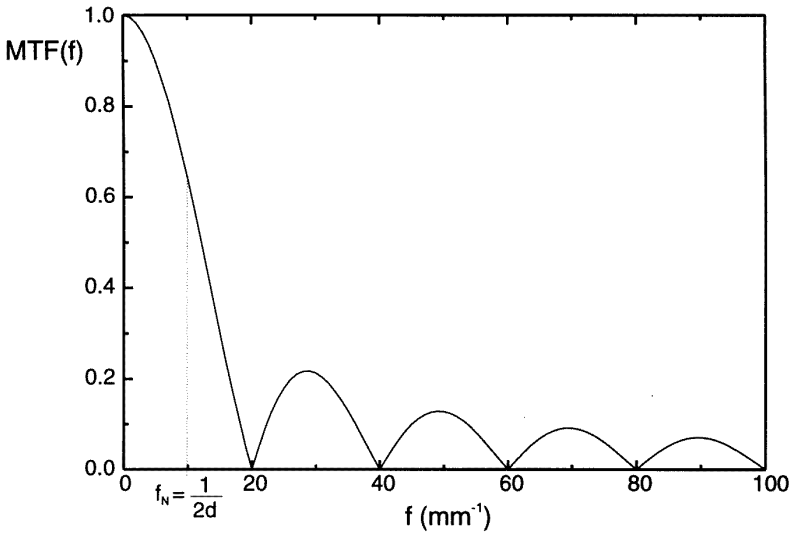

Figure 5. Effect of a 50 μm rectangular detector aperture on MTF of the image receptor. The Nyquist frequency, f_N, above which aliasing occurs is indicated.

3.5. Noise

All images generated by quanta are statistical in nature, i.e. although the image pattern can be predicted by the attenuation properties of the patient, it will fluctuate randomly about the mean predicted value. The fluctuation of the x-ray intensity follows Poisson statistics, so that the variance, σ^2, about the mean number of x-ray quanta, N_0, falling on a detector element of a given area, is equal to N_0. Interaction with the detector can be represented as a binomial process with probability of success, η, and it has been shown (Barrett and Swindell 1981) that the distribution of interacting quanta is still Poisson with standard deviation

$$\sigma = (N_0\eta)^{1/2}. \tag{2}$$

If the detection stage is followed by a process that provides a mean gain $\bar{g}$, then the 'signal' becomes

$$q = N_0\eta\bar{g} \tag{3}$$

while the variance in the signal is

$$\sigma_q^2 = N_0\eta(\bar{g}^2 + \sigma_g^2). \tag{4}$$

In general, the distribution of q is not Poisson even if g is Poisson distributed. Similarly, the effect of additional stages of gain (or loss) can be expressed by propagating this expression further (Rabbani *et al* 1987, Cunningham *et al* 1994, Yaffe and Nishikawa 1994). It is also possible that other independent sources of noise will be contributed at different stages of the imaging system. Their effect on the variance at that stage will be additive and the fluctuation will be subject to the gain of subsequent stages of the imaging system.

A complete analysis of signal and noise propagation in a detector system must take into account the spatial frequency dependence of both signal and noise. Signal transfer can be characterized in terms of the modulation transfer function, $MTF(f)$, where f is the spatial

frequency, while noise is described by the noise power or Wiener spectrum $W(f)$. Methods for calculating the Wiener spectral properties of a detector must correct for nonlinearities in the detector and must properly take into account the spatial correlation of signal and statistical fluctuation (Rabbani *et al* 1987, Cunningham *et al* 1994).

A useful quantity for characterizing the overall signal and noise performance of imaging detectors is their spatial frequency-dependent detective quantum efficiency, $DQE(f)$. This describes the efficiency in transferring the signal-to-noise ratio (squared) contained in the incident x-ray pattern to the detector output. Ideally, $DQE(f) = \eta$ for all f, but additional noise sources will reduce this value and often cause the DQE to decrease with increasing spatial frequency. $DQE(f)$ can be treated as a sort of quantum efficiency, in that when it is multiplied by the number of quanta incident on the detector, one obtains $\mathrm{SNR}^2_{out}(f)$, also known as the number of noise equivalent quanta, $NEQ(f)$, used to form the image. Typically DQE for a screen-film detector has a value on the order of 0.2 at a spatial frequency of 0 cycles/mm and this may fall to 0.05 at a few cycles/mm (Bunch *et al* 1987).

As discussed in section 4, it is important that the number of secondary quanta or electrons at each stage of the detector is somewhat greater than $N_0\eta$, to avoid having the detector noise being dominated by a 'secondary quantum sink'.

Table 1. Properties of phosphors and photoconductors used as x-ray detectors for digital radiography, including atomic number, Z, and K absorption energy, E_K, of the principal absorbing elements. Sensitivity is expressed as the energy, w, which must be absorbed to release a quantum of light in a phosphor or an electron–hole pair in a photoconductor. The fluorescent yield, ω_K, is the probability that when a K-shell photoelectric interaction occurs, there will be a fluorescent (characteristic) x-ray rather than an Auger electron given off.

Material	Z	E_K (keV)	w (eV)	ω_K (approx.)[a]
CdTe	48/52	26.7/31.8	4.4	0.85–0.88
High-purity Si	14	1.8	3.6	< 0.05
Amorphous selenium	34	12.7	50 (at 10 V $\mu\mathrm{m}^{-1}$)[b]	0.6
CsI(Tl)	55/53	36.0/33.2	19	0.87
Gd_2O_2S	64	50.2	13	0.92
BaFBr (as photostim. phosphor)	56/35	37.4/13.5	50–100[c]	0.86

[a] From Evans (1955).

[b] 7 eV (theoretical value at infinite field).

[c] Estimated by multiplying the bandgap of 8.3 eV by 3 (Klein 1968) and then 2 for the 50% efficiency of trap filling during x-ray exposure. The higher value reflects a possible additional loss of up to a factor of 2 is due to retrapping during readout.

3.6. Sensitivity

The final output from virtually all x-ray detectors is an electrical signal, so that sensitivity can be defined in terms of the charge produced by the detector (before any external amplification) per incident x-ray quantum of a specified energy. The sensitivity of any imaging system depends on η and on the primary conversion efficiency (the efficiency of converting the energy of the interacting x-ray to a more easily measurable form such as optical quanta or electric charge). Conversion efficiency can be expressed in terms of the energy, w, necessary to release a light photon in a phosphor, an electron–hole pair in a photoconductor (or semiconductor) or an electron–ion pair in a gaseous detector. Values of w for some typical detector materials are given in table 1. The limiting factor is related to the intrinsic

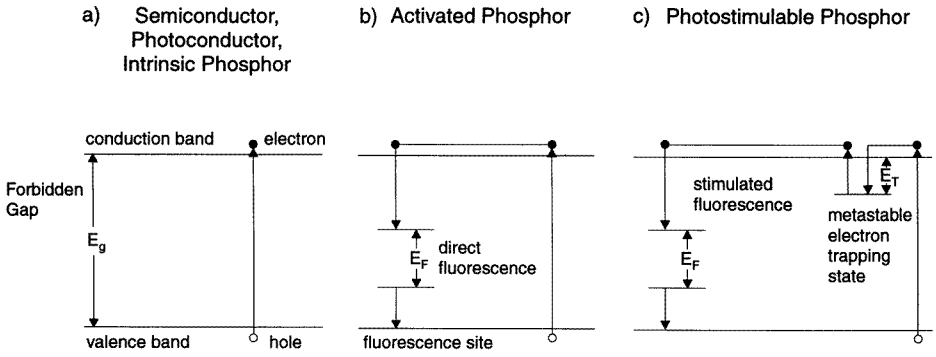

Figure 6. Energy level diagrams for crystals used in (*a*) direct conversion x-ray detectors, (*b*) conventional phosphors, (*c*) photostimulable phosphor imaging.

band structure of the solid from which the detector is made. In figure 6(*a*) the basic band structure of a crystalline material is shown. Normally the valence band is fully populated with electrons and the conduction band is empty. The energy gap governs the scale of energy necessary to release an electron–hole pair, i.e. to promote an electron from the valence band to the conduction band. However, though this energy is the *minimum* permitted by the principle of conservation of energy, this can be accomplished only for photons of energy exactly equal to the energy gap. For charged particles releasing energy (e.g. through the slowing down of high-energy electrons created by an initial x-ray interaction), requirements of conserving both energy and crystal momentum as well as the presence of competing energy loss processes require, on average, at least three times as much energy as the bandgap to release an electron–hole pair (Klein 1968). In figure 6(*b*) the situation for a phosphor is shown. In this case, the first requirement is to obtain an electron–hole pair. Subsequently, the electron returns to the valence band via a luminescence centre created by an activator added to the host material. This requires that the energy E_F of the fluorescence light must be less than the bandgap energy E_G and therefore there are further inevitable inefficiencies in a phosphor compared to a photoconductor of the same E_G.

3.7. Dynamic range

The dynamic range can be defined as:

$$DR = \frac{X_{\max}}{X_{\text{noise}}} \tag{5}$$

where $X_{\max}$ is the x-ray fluence providing the maximum signal that the detector can accommodate and X_{noise} is the fluence that provides a signal equivalent to the quadrature sum of the detector noise and the x-ray quantum noise.

While this definition describes the performance of the detector on an individual pixel basis, it is less useful for predicting the useful range of detector operation for a particular imaging task. This is because at the bottom of this range the signal-to-noise ratio (SNR) is only 1 and this is seldom acceptable. Also, it is rare to base a medical diagnosis on a single image pixel and therefore, for most objects, the SNR is based on the signal from multiple pixels. For a large object, the noise on a pixel by pixel basis can be large, but if there is integration over the object, the effective SNR will improve approximately as the square

root of the area (with some correction for correlation effects caused by unsharpness of the imaging system). We have, therefore, offered a second definition of 'effective dynamic range' which we have found useful

$$DR_{\text{eff}} = \frac{k_2 X_{\max}}{k_1 X_{\text{noise}}}. \tag{6}$$

Here, the constant k_1 is the factor by which the minimum signal must exceed the noise for reliable detection. Rose (1948) has argued that k_1 should be on the order of 4 or 5 depending on the imaging task. The constant k_2, which is dependent on the imaging task and the system MTF, reflects the improvement in SNR due to integration over multiple pixels. Effectively, this causes the dynamic range of the imaging system to increase even though the maximum signal level and the single pixel noise level have not changed. Maidment *et al* (1993) and Neitzel (1994) have analysed this problem for the case of digital mammography.

In practice, the required dynamic range for an imaging task can be decomposed into two components. The first describes the ratio between the x-ray attenuation of the most radiolucent and most radio-opaque paths through the patient to be included on the same image. The second is the precision of x-ray signal to be measured in the part of the image representing the most radio-opaque anatomy. If, for example, there was a factor of 50 in attenuation across the image field and it was desired to have 1% precision in measuring the signal in the most attenuating region, then the dynamic range requirement would be 5000. The dynamic range requirements for certain applications may exceed the capabilities of available detectors. It is often possible to reduce the requirement by employing prepatient bolusing filters to increase attenuation in lucent areas of the image and so reduce the range of intensities that must be accommodated.

The dynamic range requirements differ between imaging tasks, but some general principles for establishing the requirements of each modality can be put forward. First it is important to recognize that the x-rays are attenuated exponentially, thus an extra tenth-value layer thickness of tissue will attenuate the beam by an additional factor of 10, while the same tenth-value thickness missing will increase the x-ray fluence by a factor of 10. Thus when a mean exposure value X_{mean} for the system is established by irradiating a uniform phantom, we are interested in multiplicative *factors* above and below this mean value, i.e. X_{mean} is a geometric rather than arithmetic mean. Thus, for example in fluoroscopy, it is generally established that a range of 100:1 is useful but it is also essential to understand this range should be between $X_{\text{mean}}/10$ and $10X_{\text{mean}}$ rather than distributed in equal linear increments, i.e. between $X_{\text{mean}}/50$ and $2X_{\text{mean}}$.

In defining the range of operation for a detector, one must consider both the need for adequate x-ray fluence to achieve the desired quantum counting statistics at the low end of the range as well as detector phenomena such as saturation or 'blooming' that can occur with large signals.

3.8. Uniformity

It is important that the radiographic imaging system provide uniformity, i.e. the sensitivity be constant over the entire area of the image. Otherwise patterns that might disrupt the effective interpretation of the image may result. These patterns are sometimes referred to as 'fixed pattern noise'. In an analogue imaging system, great pains must be taken in the design and manufacture of detectors to ensure that they provide uniform response.

In a digital system, the task is much easier, because, at least over a considerable range, differences in response from element to element can be corrected. This is accomplished

by imaging an object of uniform x-ray transmission, recording the detector response and using this as a 'correction mask'. If the detector has linear response to x-rays, then the correction involves two masks—one with and one without radiation—to provide slope and intercept values for the correction of each element. If the detector response is nonlinear, then measurements must be made over a range of intensities and a nonlinear function fit to the response of each element to obtain the correction coefficients. In some detectors, non-uniformities might exist only over rows and columns of the detector rather than over individual elements. This greatly reduces the number of coefficients that must be stored.

4. Phosphor-based detector systems

Most x-ray imaging detectors employ a phosphor in the initial stage (figure 7(*a*)) to absorb the x-rays and produce light which is then coupled to an optical sensor (photodetector). The use of phosphor materials with a relatively high atomic number causes the photoelectric effect to be the dominant type of x-ray interaction. The photoelectron produced in these interactions is given a substantial fraction of the energy of the x-ray. This energy is much larger than the bandgap of the crystal (figure 6(*b*)) and, therefore, in being stopped, a single interacting x-ray has the potential to cause the excitation of many electrons in the phosphor and thereby the production of many light quanta. We describe this 'quantum amplification' as the conversion gain, g_1. For example, in a Gd_2O_2S phosphor, the energy carried by a 60 keV x-ray quantum is equivalent to that of 25 000 green light quanta ($E_g = 2.4$ eV). Because of competing energy loss processes and the need to conserve momentum, the conversion efficiency is only about 15%, so that, on average, it requires approximately 13 eV per light quantum created in this phosphor (table 1). The conversion gain is then approximately 4500 light quanta per interacting x-ray quantum.

The energy loss process is stochastic and, therefore, g has a probability distribution, with standard deviation, σ_g, about its mean value as illustrated in figure 8(*a*). Swank (1973) described this effect, and the 'Swank factor', A_s, characterizes this additional noise source. The Swank factor is calculated in terms of the moments of the distribution of g as

$$A_s = \frac{M_1^2}{M_0 M_2} \tag{7}$$

where M_i indicates the ith moment of the distribution.

The actual number of quanta produced by an interacting x-ray will also depend both on its incident energy and the mechanism of interaction with the phosphor crystal. The most likely type of interaction, the photoelectric effect, will result in both an energetic photoelectron and either a second (Auger) electron or a fluorescent x-ray quantum. The energy of fluorescence depends on the shell in which the photoelectric interaction took place. The threshold K-shell energy for these interactions is shown for some common radiographic phosphors in table 1. Also in the table is the K-fluorescence yield; the probability of emission of x-ray fluorescence, given that a K-shell photoelectric interaction has occurred. For example, K-shell interactions for the Gd in Gd_2O_2S have a threshold of 50.2 keV and produce the most intense fluorescence (92% of K-shell interactions yield these quanta) just below 43 keV. The fluorescent quanta are either reabsorbed in the phosphor or escape. In either case, if they are not absorbed locally, the apparent energy deposited in the phosphor from the x-ray quantum is reduced, giving rise to a second peak in the distribution with a lower value of g. The effect of fluorescence loss is to broaden the overall distribution of g (figure 8(*b*)), thus decreasing A_s and causing an increase in σ_g.

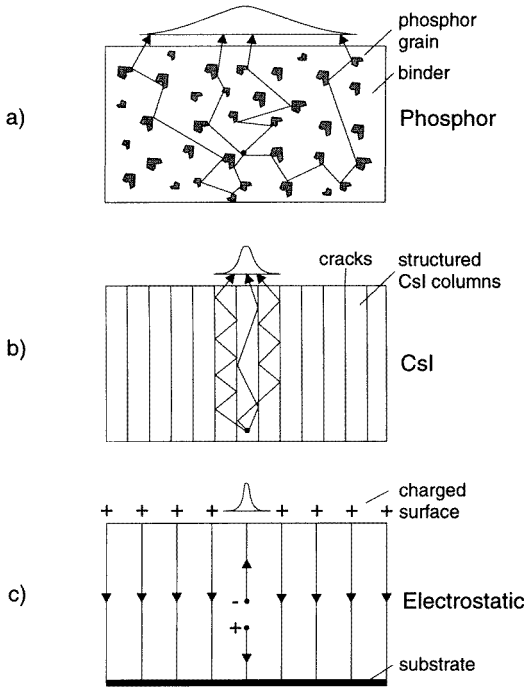

Figure 7. Three types of detector structures: (*a*) settled phosphor, (*b*) columnar CsI phosphor and (*c*) direct x-ray convertor with charge collection in an electric field. A hypothetical line-spread function of each system is shown.

There are both advantages and disadvantages in imaging with an x-ray spectrum that exceeds the K edge of the phosphor. Clearly, the value of η increases, but the 'Swank noise' does also. In addition, deposition of energy from the fluorescence at some distance from the point of initial x-ray interaction causes the point spread function of the detector to increase, resulting in decreased spatial resolution.

After their formation, the light quanta must successfully escape the phosphor and be effectively coupled to the next stage for conversion to an electronic signal and readout. It is desirable to ensure that the created light quanta escape the phosphor efficiently and as near as possible to their point of formation.

Figure 9 illustrates the effect of phosphor thickness and the depth of x-ray interaction on spatial resolution of a phosphor detector. The probability of x-ray interaction is exponential so that the number of interacting quanta and the amount of light created will be proportionally greater near the x-ray entrance surface.

While travelling within the phosphor, the light will spread—the amount of diffusion being proportional to the path length required to escape the phosphor. The paths of most optical quanta will be shortest if the photodetector is placed on the x-ray entrance side of the phosphor. It is usually more practical, however, to record the photons which exit on the opposite face of the phosphor screen, i.e. those which have had a greater opportunity to spread. In addition, if a phosphor layer is made thicker to improve quantum efficiency, the spreading becomes more severe. This imposes a fundamental compromise between spatial resolution and η. Methods to collect the emission from the entrance side of the phosphor

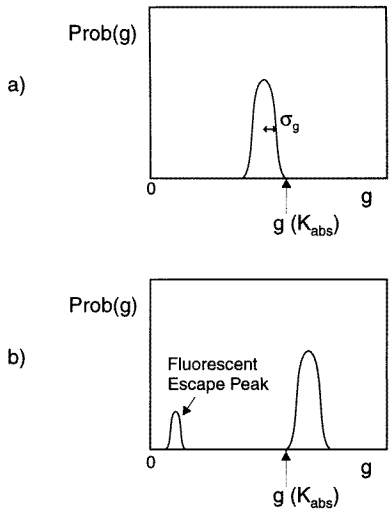

Figure 8. Effect of fluorescence loss on the distribution of g_1 for monoenergetic x-rays. The value of g corresponding to conversion of x-rays at the K absorption edge energy is shown on the abscissa. (*a*) For x-rays of energy below the edge, there is a single distribution of the number of light quanta about the mean value, $\bar{g_1}$ while for energies above the absorption edge (*b*) there is a bimodal distribution, where the upper peak corresponds to total absorption of the incident x-ray, while the lower peak corresponds to conversion of the energy of the incident x-ray minus the energy of the fluorescent x-ray that has escaped the phosphor.

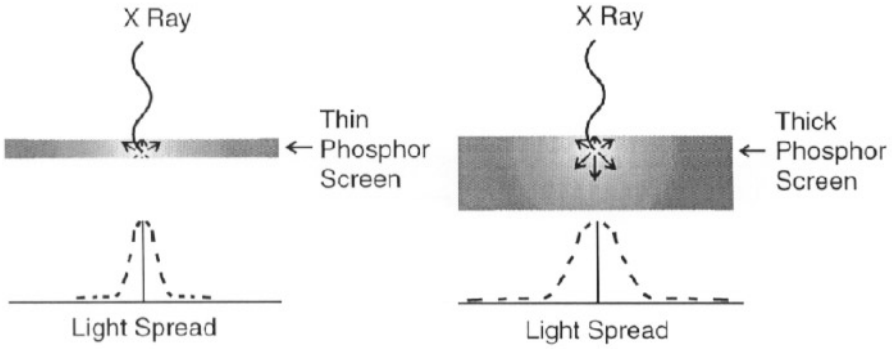

Figure 9. Phosphor thickness, depth of x-ray interaction and line spread function: (*a*) thin screen, (*b*) increased line spread function for a thicker screen. In either case, spatial resolution would be improved if it were possible to measure the signal from the face of the detector on which the x-rays are incident.

or to channel the optical photons out of the phosphor without spreading would significantly improve phosphor performance.

Phosphor screens are typically produced by combining 5–10 μm diameter phosphor particles with a transparent plastic binder (figure 7(*a*)). The phosphor grains are highly scattering particles due to the high refractive index of phosphors compared with that of the binder. The scattering is sufficiently intense to cause the layer to be turbid: i.e. the

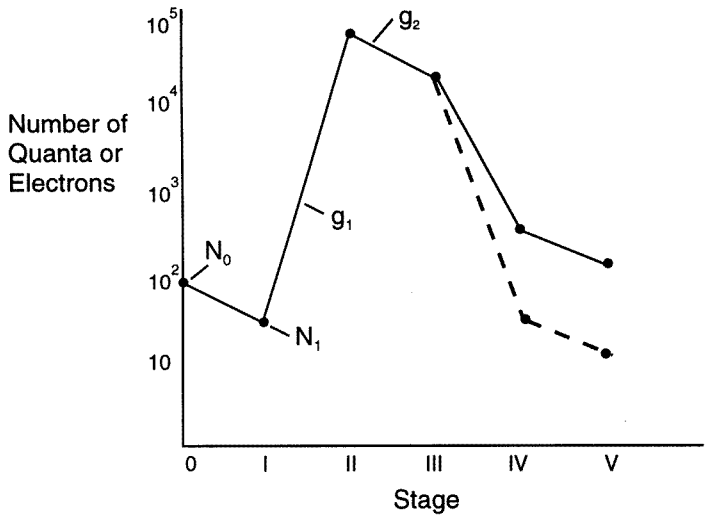

Figure 10. Number of quanta or charges at different stages in an imaging system: Full curve, x-ray limited; broken curve, inadequate conversion and/or coupling yields a secondary quantum sink.

propagation of photons can be considered to be diffusive. This results in a limit to the lateral spreading of the light to the order of the thickness of the layer. Other optical effects can also be used to control the imaging properties of the screen—for example a reflective backing helps to increase the amount of light escaping the opposite side of the screen, but at the cost of increased lateral spread, and hence reduced resolution. Typically, without the backing, fewer than one-half of the created light quanta escape the phosphor on the side facing the photodetector and are potentially available to be recorded. Light-absorbing dye can also be added to the screen to enhance the resolution, but this results in a loss of signal. These optical techniques affect sensitivity, spatial resolution and (through their influence on the Swank factor (Drangova and Rowlands 1986)) the noise properties of the detector.

It should also be noted that the packing factor of phosphor particles in the screen may be of the order of 50% by volume. When calculations of η are made, the reduction of effective attenuation coefficient due to the binder must be considered.

Figure 10 illustrates the propagation of signal through the various energy conversion stages of an imaging system. In the diagram, N_0 quanta are incident on a specified area of the detector surface (stage 0). A fraction of these, given by the quantum detection efficiency, η, interact with the detector (stage I). In a perfect imaging system η would be equal to 1.0. The mean number, N_1, of quanta interacting represents the 'primary quantum sink' of the detector. The fluctuation about N_1 is $\sigma_{N1} = (N_1)^{1/2}$. This defines the SNR of the imaging system which increases as the square root of the number of quanta interacting with the detector.

Regardless of the value of η, the maximum SNR of the imaging system will occur at this point and if the SNR of the imaging system is essentially determined there, the system is said to be *x-ray quantum limited* in its performance. However, the SNR will, in general, become reduced in passage of the signal through the imaging system because of losses and additional sources of fluctuation.

To avoid losses that can occur at subsequent stages, it is important that the detector

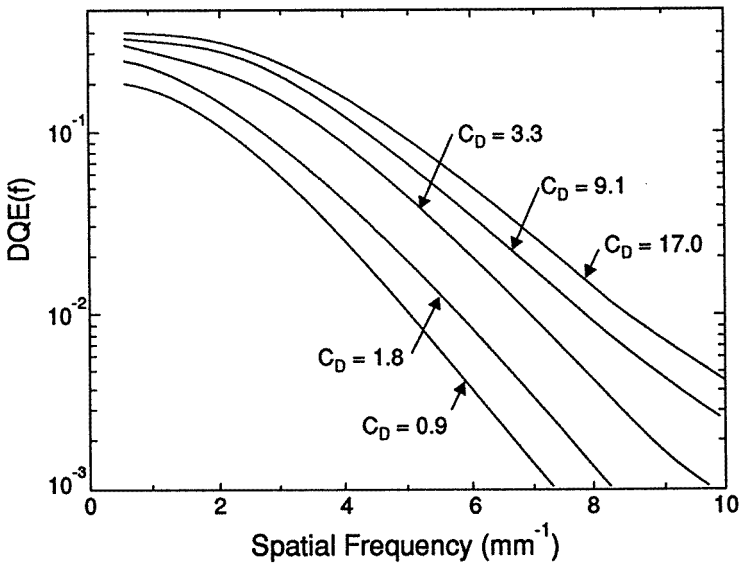

Figure 11. Effect of optical coupling efficiency on $DQE(f)$ of a phosphor–fibre optic–CCD detector. C_D is the number of electrons produced in the CCD per x-ray interacting in the phosphor. (From Maidmont and Yaffe 1994.)

provide adequate quantum gain, g_1 directly following the initial x-ray interaction. Stages II and III illustrate the processes of creation of many light photons from a single interacting x-ray (often referred to as conversion gain) and the escape of quanta from the phosphor with mean probability g_2. Here, light absorption, scattering and reflection processes are important.

Further losses occur in the coupling of the light to the photodetector which converts light to electronic charge (stage IV) and in the spectral sensitivity and optical quantum efficiency of the photodetector (stage V). If the conversion gain of the phosphor is not sufficiently high to overcome these losses and the number of light quanta or electronic charges at a subsequent stage falls below that at the primary quantum sink, then a 'secondary quantum sink' is formed. In this case the statistical fluctuation of the light or charge at this point becomes an additional important noise source. Even when an actual secondary sink does not exist, a low value of light or charge will cause increased noise. This becomes especially important when a spatial-frequency-dependent analysis of SNR is carried out and, as discussed earlier, its effect is to cause reduction of the detective quantum efficiency with increasing spatial frequency. Figure 11 illustrates the effect of optical coupling efficiency of light from a phosphor to a photodetector on $DQE(f)$ for an optically coupled system (Maidment and Yaffe 1994).

As illustrated in figure 12, there are several approaches for coupling a phosphor to a photodetector. Possibly the simplest involves the use of a lens and/or mirror system (figure 12(a)) to collect light emitted from the surface of the phosphor material and couple it to either a conventional video camera (see figure 18) or to a CCD camera. The operation of these cameras is discussed briefly later in this article.

Because the size of available photodetectors such as CCDs is limited from manufacturing considerations to a maximum dimension of only 2–5 cm, it is often necessary to demagnify

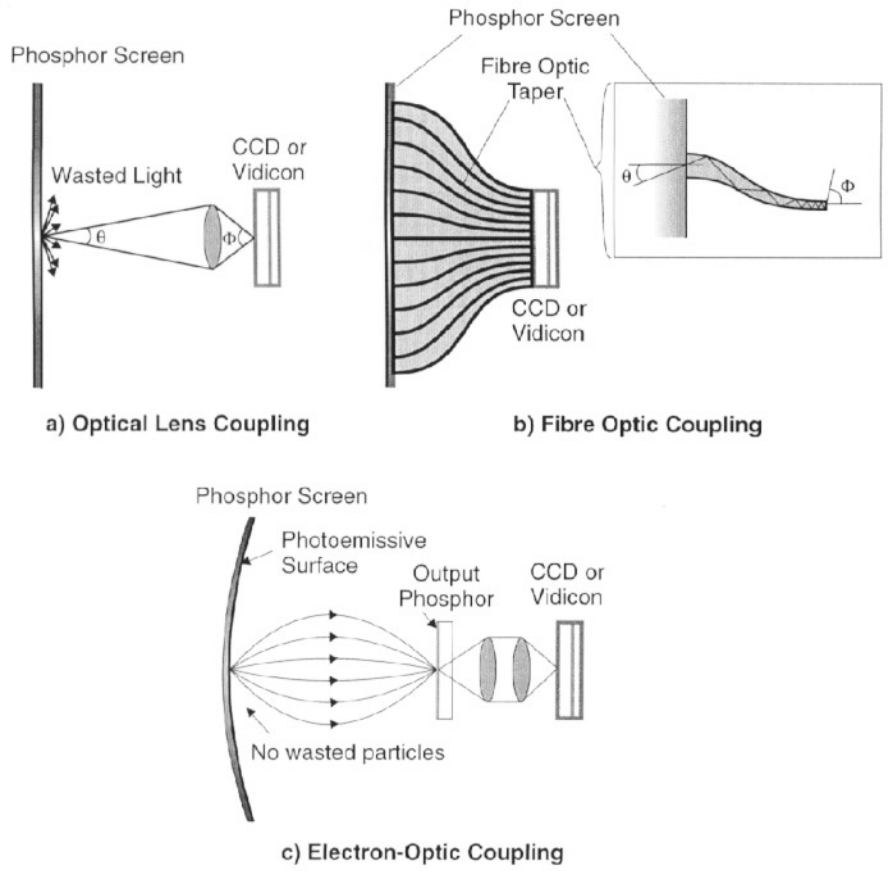

Figure 12. Methods to couple a phosphor to a photodetector: (*a*) lens, (*b*) fibre optic, (*c*) direct coupling to a photocathode whose emission is electrostatically collected.

the image from the phosphor to allow coverage of the required field size in the patient (Karellas *et al* 1992). The efficiency of lens coupling is determined largely by the solid angle subtended by the collecting optics. For a single lens system, the coupling efficiency is given by (Miller 1971, Maidment and Yaffe 1996)

$$\xi = \frac{\tau}{4F^2(m+1)^2} \tag{8}$$

where τ is the optical transmission factor for the lens, F is the 'f-number' of the lens (ratio of the focal length to its limiting aperture diameter) and m is the demagnification factor from the phosphor to the photodetector. For a lens with $F = 1.2$, $\tau = 0.8$ and $m = 10$, ξ will be 0.1%. Because of this low efficiency, the SNR of systems employing lens coupling is often limited by a secondary quantum sink, especially in such applications as radiotherapy portal imaging where the demagnification factor is large (Munro *et al* 1990). On the other hand, lenses are successfully used for coupling in situations where m is small and g_1 is large (Roehrig *et al* 1994).

It is also possible to use fibre optics to effect the coupling. These can be in the form of fibre optic bundles (figure 12(*b*)), where optical fibres of constant diameter are fused to form a light guide. The fibres form an orderly array so that there is a one-to-one correspondence

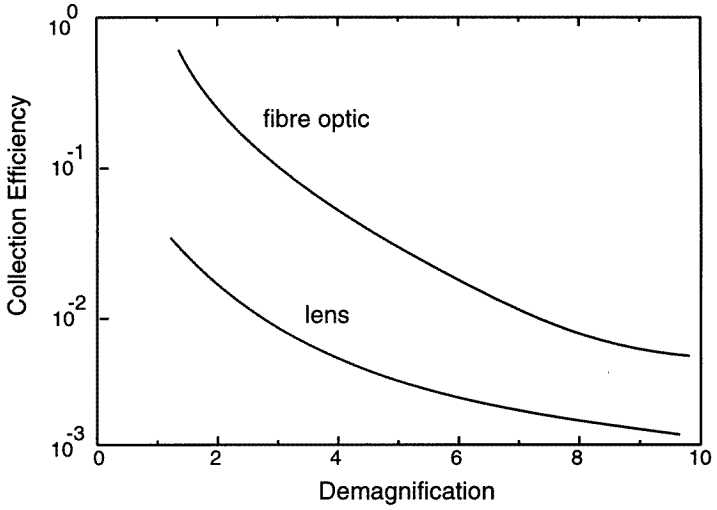

Figure 13. Comparison of the efficiency of lens and fibre optic coupling between a phosphor and CCD. The f number of the lens is 1.2. (Modified from Hejazi and Trauernicht 1996.)

between the elements of the optical image at the exit of the phosphor and at the entrance to the photodetector. To accomplish the required demagnification, the fibre optic bundle can be tapered by drawing it under heat. While facilitating the construction of a detector to cover the required anatomy in the patient, demagnification by tapering also reduces coupling efficiency by limiting the acceptance angle at the fibre optic input. A simplified expression for the coupling efficiency of a fibre optic taper is

$$\xi = \alpha\tau(\theta)\frac{NA^2}{m^2} \tag{9}$$

where α is the fraction of the entrance surface that comprises the core glass of the optical fibres, $\tau(\theta)$ is the transmission factor for the core glass, NA is the numerical aperture of the untapered fibre and m is the demagnification factor due to tapering. For example, a taper with 10 times demagnification ($m = 10$), with $\alpha = 0.8$, $\tau = 0.9$ and $NA = 1.0$, has an efficiency of 0.7%, about seven times higher than a lens with $F = 1.2$ with the same demagnification factor and about 2.5 times higher than a lens with $F = 0.7$. It should be noted that for both lenses and fibre optics, the transmission efficiency is dependent on the angle of incidence, θ of the light and, therefore, a complete analysis involves an integral of the angular distribution of emission of the phosphor over θ. A comparison of the efficiency of lens versus fibre optic coupling is shown in figure 13 (Hejazi and Trauernicht 1996).

Systems of both designs are used in cameras with a small field of view for digital mammography, both for guiding needle biopsy and for localization of suspicious lesions. In such applications, much lower demagnification, typically two times, is used, resulting in acceptable coupling efficiency. By abutting several camera systems to form a larger matrix, a full-field digital breast imaging system can be constructed (Feig and Yaffe 1995), while still maintaining a low value of m and thus an adequate value of g_1 to avoid a secondary quantum sink.

Fibre optic bundles are subject to geometric distortion which must be minimized. To maintain high resolution, the crosstalk of signal between fibres must be controlled and this is accomplished, in part, by the use of extramural absorber (EMA), i.e. an optically attenuating

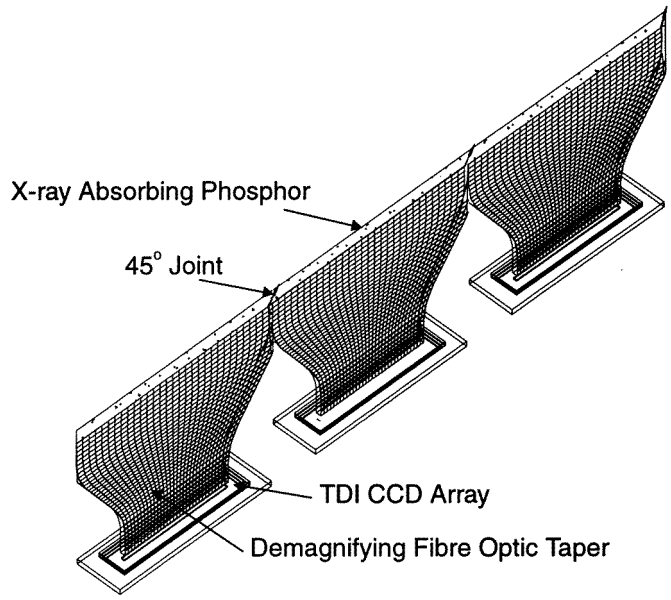

Figure 14. Phosphor–fibre optic–CCD detector assembly for slot-scanned digital mammography. Detector input dimensions are 24 cm × 3.2 mm.

material incorporated between individual fibres in the bundle to absorb light that escapes from the fibres or that directly enters the fibre cladding material on the entrance surface of the bundle.

5. Scanned-beam acquisition

One way of overcoming the size and cost limitations of available high-resolution photodetectors in producing a large imaging field is to create an image receptor that is essentially one dimensional and acquires the second dimension of the image by scanning the x-ray beam and detector across the patient. In principle this could be done by employing a single line detector and a very highly collimated slit beam of x-rays. This is extremely inefficient because of the poor utilization of the output of the x-ray tube. Most of the x-rays would be removed by the collimator and a full scan would impose an enormous heat loading on the tube. It is possible to improve the efficiency of such systems tremendously by employing a multiline or 'slot' detector. Here, the x-ray beam would extend across the full image field in one dimension but would be narrow (e.g. 3–15 mm) in the other. In our group, we have used such a design to construct a digital mammography system (Nishikawa *et al* 1987, Yaffe 1993). This is composed of a strip of phosphor material with dimensions 3.2 mm × 240 mm. This is coupled to three fibre optic tapers which are abutted with mitre joints at their input surfaces as shown in figure 14. Their taper ratio of 1.58:1 provides demagnification with acceptable light collection efficiency for this application while providing a space between the tapers at the output to accommodate the outer non-active regions of three CCD arrays, which are bonded directly on the tapers. Acquisition takes place in time delay integration (TDI) mode in which the x-ray beam is activated continuously during the image scan and charge collected in pixels of the

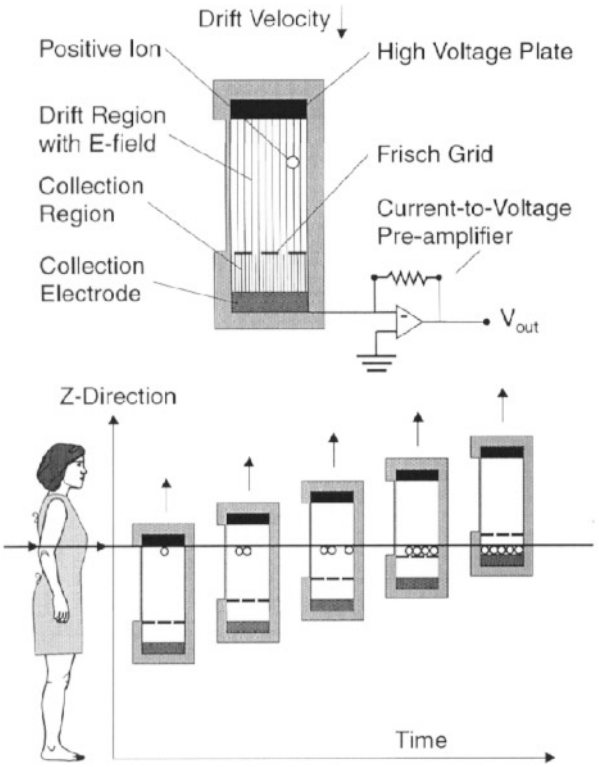

Figure 15. Kinestatic gaseous ionization imaging detector employing the TDI principle.

CCDs is shifted down CCD columns at a rate equal to but in the opposite direction as the motion of the x-ray beam and detector assembly across the breast. The collected charge packets remain essentially stationary with respect to a given projection path of the x-rays through the breast and the charge is integrated in the CCD column to form the resultant signal. When the charge packet has reached the final element of the CCD, it is read out on a transfer register and digitized. The CCD array can be cooled using thermoelectric devices to reduce noise and increase the dynamic range of the image receptor as necessary.

Another (non-phosphor) TDI approach, called 'kinestatic imaging' has been demonstrated by DiBianca and Barker (1985) and Wagenaar and Terwilliger (1995) where the imaging detector is a gaseous ionization chamber in which the charge signal is collected by a large number of linear electrode strips which run parallel to the direction of propagation of the x-ray beam (figure 15). This provides one-dimensional spatial localization. By carefully controlling the drift velocity of the ions toward the collectors in an electric field and synchronizing this with the motion of the detector assembly in the opposite direction, a TDI acquisition can be accomplished. The value of η for this detector is determined by the type of gas used, its pressure, the thickness of the detector along the direction of x-ray travel and the window attenuation. Spatial resolution is determined by the homogeneity of the ion drift speed, ion diffusion and the spacing between the collecting electrodes.

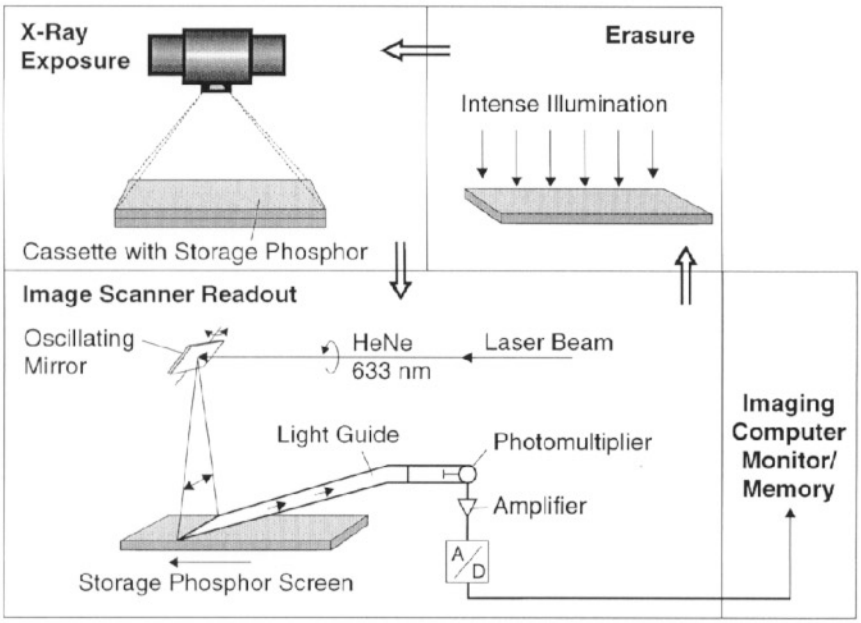

Figure 16. Schematic representaion of a photostimulable phosphor digital radiography system.

6. Photostimulable phosphors

Probably the most successful detectors for digital radiography to date have been photostimulable phosphors, also known as storage phosphors. These phosphors are commonly in the barium fluorohalide family, typically $BaFBr:Eu^{2+}$, where the atomic energy levels of the europium activator determine the characteristics of light emission. X-ray absorption mechanisms are identical to those of conventional phosphors. They differ in that the useful optical signal is not derived from the light that is emitted in prompt response to the incident radiation, but rather from subsequent emission when electrons and holes are released from traps in the material (Takahashi *et al* 1984, von Seggern *et al* 1988). The initial x-ray interaction with the phosphor crystal causes electrons to be excited (figure 6(*c*)). Some of these produce light in the phosphor in the normal manner, but the phosphor is intentionally designed to contain traps which store the charges. By stimulating the crystal by irradiation with red light, electrons are released from the traps and raised to the conduction band of the crystal, subsequently triggering the emission of shorter-wavelength (blue) light. This process is called photostimulated luminescence. Early analysis of these systems was provided by Hillen *et al* (1987) and a comparison with screen–film systems was performed by Sanada *et al* (1991). Recent reviews of photostimulable phosphor imaging were presented by Kato (1994) and Bogucki *et al* (1995).

In the digital radiography application, the imaging plate is positioned in a light-tight cassette or enclosure, exposed and then read by raster scanning the plate with a laser to release the luminescence (figure 16). The emitted light is collected and detected with a photomultiplier tube whose output signal is digitized to form the image.

The energy levels in the crystal are critical to the effective operation of the detector (figure 6(*c*)). The energy difference between the traps and the conduction band E_T must be

small enough so that stimulation with laser light is possible, yet sufficiently large to prevent random thermal release of the electron from the trap. Finally, the energetics should provide for a wavelength of the emitted light that can be efficiently detected by a photomultiplier and for adequate wavelength separation between the stimulating and emitted light quanta to avoid contaminating the measured signal. The electrons liberated during irradiation either produce light promptly or are stored in traps. Because the 'prompt' light is not of interest in this application, the efficiency of the storage function can be improved by increasing the probability of electron trapping. On the other hand, when these electrons are released by the stimulating light during readout, the probability of their being retrapped instead of producing light, would then be higher, so that the efficiency of readout would be reduced. The optimum balance occurs where the probabilities of an excited electron being retrapped or stimulating fluorescence are equal. This causes the conversion efficiency to be reduced by a factor of four compared to the same phosphor without traps, i.e. a factor of two from the prompt light given off during x-ray exposure and another factor of two from unwanted retrapping of the electrons during readout.

In addition, the decay characteristics of the emission must be sufficiently fast such that the image can be read in a conveniently short time while capturing an acceptable fraction of the emitted energy. In practice, depending on the laser intensity, the readout of a stimulable phosphor plate yields only a fraction of the stored signal. This is a disadvantage with respect to sensitivity and readout noise, but it can be helpful by allowing the plate to be 'pre-read', i.e. read out with only a small part of the stored signal, to allow automatic optimization of the sensitivity of the electronic circuitry for the main readout.

6.1. Strengths and limitations of stimulable phosphors

The photostimulable phosphor is an excellent detector for digital radiography in that, when placed in a cassette, it can be used with conventional x-ray machines. Large-area plates are conveniently produced, and because of this format, images can be acquired quickly. The plates are reusable, have linear response over a wide range of x-ray intensities, and are erased simply by exposure to a uniform stimulating light source to release any residual traps.

One limitation of this type of detector is that because the traps are located throughout the depth of the phosphor material, the laser beam providing the stimulating light must penetrate into the phosphor. Scattering of the light within the phosphor causes release of traps over a greater area of the image than the size of the incident laser beam. This results in loss of spatial resolution, which is aggravated if the plate is made thicker to increase η. An ideal solution to this problem would be a phosphor which was non-scattering for the stimulating light and both non-scattering and non-absorbing for the emitted light. Limitations also arise primarily from the readout stage. This is mechanically complex, and efficient collection of the emitted light requires great attention to design. This can result in a secondary quantum sink, especially at high spatial frequencies, causing a reduction of $DQE(f)$.

In practice, stimulable phosphor systems are widely used for both emergency and bedside radiography, where the variable readout sensitivity allows for compensation for under and overexposure problems often experienced with screen-film radiography because it is often not possible to employ automatic exposure control in these applications. As well, this technology has been implemented both in the form of portable cassettes which are carried between the x-ray unit(s) and a central reader and also in dedicated units incorporating the plates, the reader and an erasing light source.

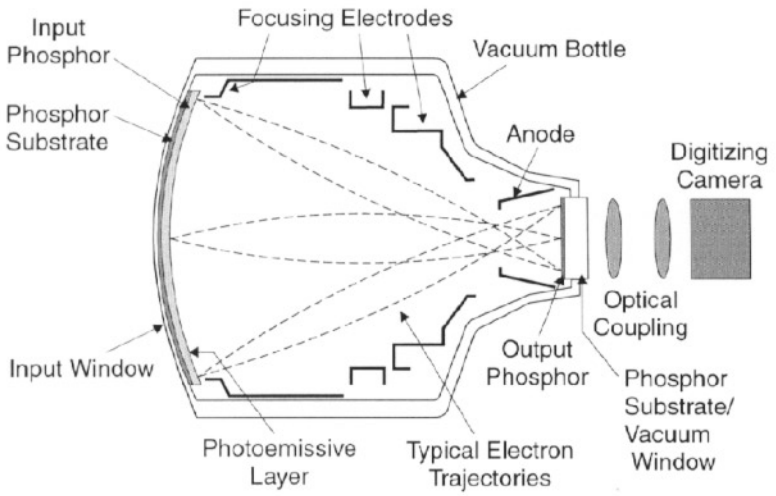

Figure 17. Image intensifier-based digital radiography system.

7. Image intensifier based detectors

Image intensified fluoroscopy is currently the only dose-efficient x-ray procedure that allows real-time visualization and interaction. The resulting real-time images are usually displayed using a video system (conventional or CCD) optically coupled to the x-ray image intensifier. Radiographs or sequences of radiographs are obtained during fluoroscopic procedures by recording XRII output by means of a small-format (photofluorographic) or ciné camera that receives the intensifier image via an optical splitter. More recently, instant radiography and instant ciné have been made possible by digitization of the video signal.

An image intensifier (XRII) digital radiography system is shown schematically in figure 17. This resembles the imaging chain used in fluoroscopy, with the exception that the video camera is capable of integrating the signal, thus facilitating digitization of the optical image from the XRII. The XRII (DeGroot 1994) absorbs the incident x-ray image, amplifies it in an essentially noise-free manner and outputs it as an optical image which is then distributed by lenses to the video camera (Rowlands 1994).

X-rays are converted to light in the large input phosphor screen typically of 12.5 cm to 40 cm in diameter. The fluorescence illuminates a photocathode evaporated directly on the phosphor and liberates electrons. The electrons are accelerated through a large potential difference (typically 25 kV) and electrostatically focused by the electrodes onto a small (2.5 cm diameter) output phosphor.

The input window is necessary to preserve the vacuum within the intensifier. It should be as transparent to x-rays as possible to avoid loss of image-forming quanta and to minimize scattering in the window which causes loss of contrast due to *veiling glare*. Initially input windows were made of glass but they are now generally metallic—convex aluminium or concave titanium.

The function of the input phosphor is to provide a high value of η and g_1 and to convey the light in as sharp an image as possible to the photocathode. CsI(Na) is universally used for this purpose (DeGroot 1994). Typically, thicknesses of 300–400 μm are employed. Its relatively high effective atomic number and high packing density lead to good quantum

detection efficiency in the diagnostic energy range. However, the unique advantage of CsI is that it can be evaporated in such a way that it acts as a fibre optic light guide. In figures 3 and 4 we compare η for CsI with that of screens made of various phosphors and to photoconductor detectors (see also Vosburg *et al* 1977).

The purpose of the photocathode is to convert light photons to electrons efficiently. The greatest efficiency is obtained when the spectral sensitivity of the photocathode is matched to the phosphor spectrum. The photocathode is extremely sensitive to contamination so it has to be made *in situ*, within the otherwise completed XRII after a very high vacuum has been established. The vacuum has to be maintained continuously thereafter.

An important factor in the achieving of gain within an XRII is the 25 keV energy each electron released from the photocathode receives from the electrostatic field before striking the output phosphor. Gain is also achieved by electronic image demagnification. The demagnification factor of any XRII can be changed by appropriate modification of the relative potentials applied to each electrode. The gain can be reduced, without change of field size, by decreasing all the applied voltages in the same proportion.

The function of the output phosphor is to convert the incident electron image to a visible light image. It should do this with the greatest possible efficiency and with the least blurring. The inner surface of the phosphor layer is overlaid by a thin, opaque, layer of aluminium which helps to maintain stable electrostatic operating conditions and prevent light from the output phosphor illuminating the photocathode layer on the input phosphor. A major problem arising in the output phosphor is veiling glare through halation, where the light intended to be emitted to the imaging lens instead gets caught within the glass substrate of the phosphor and can re-enter the phosphor layer.

There are great advantages inherent in the design of the XRII which help to make the operation of XRII-based imaging systems x-ray quantum limited. First, the intimate coupling of the phosphor and photocathode provides much higher collection efficiency of the light than with lens or fibre optic methods. Secondly, as shown in figure 12(*c*), the collection and focusing of emitted electrons by the electrostatic field is also very efficient and these two factors outweigh any inefficiency of the photocathode. Thirdly, the acceleration of the electrons within the tube provides a high gain which more than compensates for subsequent losses in the imaging system. Finally, the demagnification of the image in the tube allows efficient lens coupling to the next stage, generally a video camera.

7.1. Video camera

The video camera is optically coupled to the output of the XRII. The characteristics of video cameras are dominated by the characteristics of the optical sensor chosen. For example, the vidicon used in many fluorososcopic video cameras employs a light sensitive *target* made of low-density antimony trisulphide (Sb_2S_3). Other photoconductors with different properties are also available. The Plumbicon utilizes a PbO target, while the target of the Saticon is composed of amorphous selenium. These cameras have reduced lag compared to the vidicon, making them more suitable for applications where good temporal response is important such as digital angiography. A comprehensive review of video camera tube design and the emergence of the vidicon as the dominant type is provided by McGee (1979). All modern video sensors store charge representing the image at each pixel *continually* and over the whole active area *simultaneously* (i.e. the pixels sense light in parallel). Parallel detection is essential to a sensitive camera, but a practical system is usually read out in pixel serial form.

Figure 18 illustrates the basis of operation of the vidicon tube camera. Vidicons are

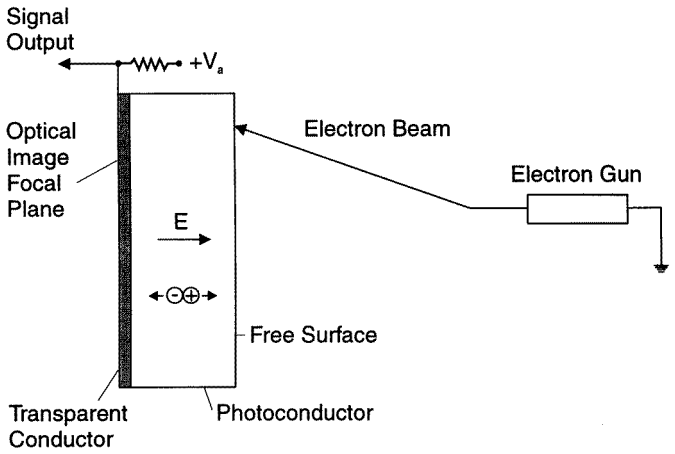

Figure 18. Operating principle of vidicon camera tube.

vacuum tube devices in which an electron beam scans the target and continually restores the free surface to the potential of the cathode of the electron gun, conventionally regarded as ground (Thompsett 1979). The illuminated side of the target is maintained at a potential V_a through a transparent electrode. Thus V_a appears across the target layer, giving rise to the electric field, E. The target is photoconductive, i.e. an excellent insulator in the dark, but readily allowing the passage of charge carriers (electrons and holes) freed by the action of light. The electric field, E, within the photoconductor causes electrons to drift to the transparent electrode while holes are drawn to the free surface. Thus a positive latent charge image forms on the free surface of the illuminated target.

Readout of the latent image is performed by the scanning electron beam. During the time the beam dwells on a particular pixel, a charge equal to the latent image charge at that pixel flows from the beam to the target to restore the target to ground potential. A preamplifier connected to the target forms the video signal from this current. The scanning pattern must be highly uniform to avoid geometrical distortion and signal distortion (shading).

X-ray noise generated in the XRII and transferred optically by the sensor (σ_x^2) is modified by the MTF of the XRII tube, the coupling optics and the video sensor. However, there are other sources of noise generated further along the imaging chain and so are independent of these transfer functions. In well-designed vidicon cameras the only significant noise of this type is amplifier noise, (σ_A^2) most of which arises in the first stage of the preamplifier. The spectrum of the amplifier noise is 'triangular' or peaked at higher spatial frequencies and thus x-ray noise is dominant at low frequencies and amplifier noise at high frequencies. The level of σ_x^2 with respect to σ_A^2 is affected by the setting of the optical aperture of the video camera. The noise in a vidicon arises in the preamplifier, not the tube itself. There is a passive contribution from the capacitance to ground of the target but this is dependent solely on the tube design and independent of the photoconductor type. Arnold and Scheibe (1984) have published the results of an investigation of the noise of XRII systems with video cameras for the application to digital subtraction angiography.

Fluoroscopic cameras have to be modified for application to digital radiography. It is desirable that the camera have a linear response to the incident light, i.e. $\gamma = 1.0$, where γ is the slope of the graph of the logarithm of video output versus the logarithm of light intensity. Two disadvantages of the Sb_2S_3 vidicon for digital radiography applications are

its nonlinearity with light intensity ($\gamma \sim 0.7$) as well as an excessively large dark current. Plumbicon and Saticon tubes have essentially linear response to light intensity and negligible dark current and are, therefore, preferred for digital radiography.

Digital radiography video cameras are typically operated in pulse progressive readout (PPR) mode (Baily 1980). In PPR, prior to the x-ray pulse the video camera tube target is 'scrubbed' by continuous scanning. When initiating an x-ray exposure, the camera is 'blanked' (i.e. the scanning electron beam current is reduced to zero at the end of the next full frame of scrubbing) and then the pulsed x-ray exposure is made. The image is then progressively read off the video camera target by restoring the beam current at the beginning of the video frame and digitizing at a rate and bandwidth compatible with the required image quality.

The sensitivity of the digital camera, and therefore the amount of radiation used per frame, can be controlled by varying the efficiency of optical coupling between the intensifier and camera tube by the adjustment of an optical diaphragm. Opening the diaphragm will permit utilization of reduced exposure per frame which will increase the quantum noise. Typical PPR systems are 'dose efficient' in the range from 10–100 μR/frame (25 cm mode) and 20–200 μR/frame (15 cm mode) (Rowlands *et al* 1989).

By using a video camera in PPR mode it is possible to capture images efficiently over a wide range of x-ray exposure times. Video systems with 1024×1024 pixels, coupled to intensifiers of 15 or 25 cm input diameter have been shown to be capable of clinical image quality equivalent to that of 100 mm photofluorography (Hynes *et al* 1989). Digital correction of vignetting and structural mottle, coupled with automatic image enhancement algorithms, can further improve the acceptability of PPR digital images. For general radiography, larger intensifier fields are necessary with increased matrix sizes to maintain resolution.

8. Charge-coupled devices (CCDs)

The CCD has been discussed above in relation to its use as a readout device for phosphor-based detectors. More detail on CCD operation is provided here. The charge-coupled device was developed in 1970 (Boyle and Smith 1970). Because of its compactness and dynamic range characteristics, it has virtually replaced the vacuum camera tube in commercial and home video and it has found many applications in digital imaging. This has largely come about due to the development of techniques for producing extremely pure crystalline silicon and for very large scale integration (VLSI).

CCDs are particularly well suited to digital radiography because of their high spatial resolution capability, wide dynamic range and high degree of linearity with incident signal. They can be made sensitive to light or to direct electronic input. A CCD is an integrated circuit formed by depositing a series of electrodes, called 'gates' on a semiconductor substrate to form an array of metal-oxide-semiconductor (MOS) capacitors (figure 19). By applying voltages to the gates, the material below is depleted to form charge storage 'wells'. These store charge injected into the CCD or generated within the semiconductor by the photoelectric absorption of optical quanta. If the voltages over adjacent gates are varied appropriately, the charge can be transferred from well to well under the gates, much in the way that boats will move through a set of locks as the potentials (water heights) are adjusted.

In area CCDs, a 'frame transfer' system (figure 20(*a*)) is employed to obtain rapid readout. Charge is initially accumulated on 'detector' pixels and then transferred to an array of 'storage' pixels from which the signal can be read line by line. Alternatively, 'interline readout' CCDs (figure 20(*b*)) have a line of optically shielded storage and transfer

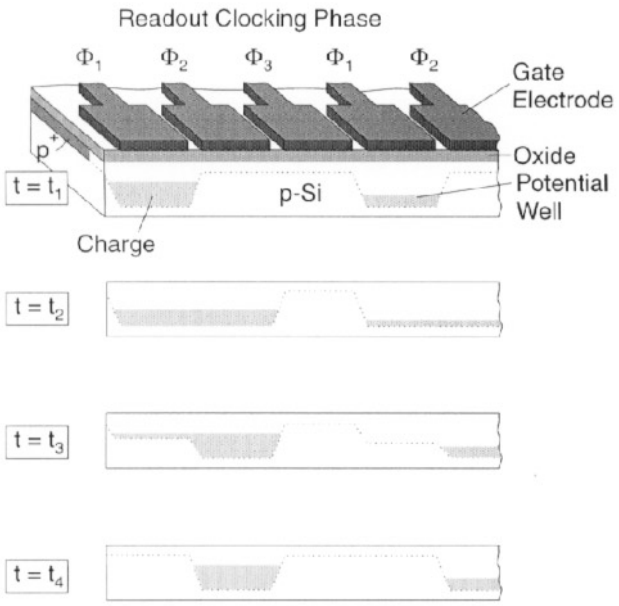

Figure 19. Structure of a CCD array, illustrating motion of stored charge in one direction as the potential wells are adjusted under control of the gate electrode voltages.

pixels adjacent to each column of detector elements. The charge is rapidly unloaded into the storage column, freeing the detector elements to accumulate new signal, and transferred down the storage column elements to a master output register which sequentially receives signal from each storage column.

These modes of operation are used for the small-format-area imagers which may be coupled to XRIIs or to phosphors through fibre optics or lenses. Although they provide rapid readout, these systems require a storage area that is approximately equal to the active photodetector area. In the case of interline devices, because the storage area is immediately adjacent to the detector columns, this may cause the effective fill factor of the detector to be reduced. Area format CCDs are available in sizes varying from 256×256 pixels or less to 2048×2048 or more. However, real-time readout (30 frames/s) is currently restricted to devices of 1000×1000 pixels or less.

For scanning systems, as discussed above, it is usually more practical to operate the CCD in time delay integration (TDI) mode (figure 20(*c*)). Here, a storage section is not required as the charge is simultaneously integrated and shifted down the CCD detector columns toward the horizontal readout register. This type of analogue integration is desirable as it is relatively noise free. In addition, because all of the detector elements in a column contribute to each image pixel imaged by that column, the image produced by TDI is relatively insensitive to a few pixels in the column that may suffer from abnormally low or high sensitivity.

In any CCD, the charge is transferred 'bucket brigade' style over many adjacent elements. It is, therefore, critical that the efficiency of each transfer is extremely high. Lack of transfer efficiency can cause a serious loss of spatial resolution in the detector. If the signal must be shifted across n elements and the efficiency per transfer is ε, then the overall charge transfer efficiency is ε^n . Even if ε is 0.999, the efficiency falls to 90%

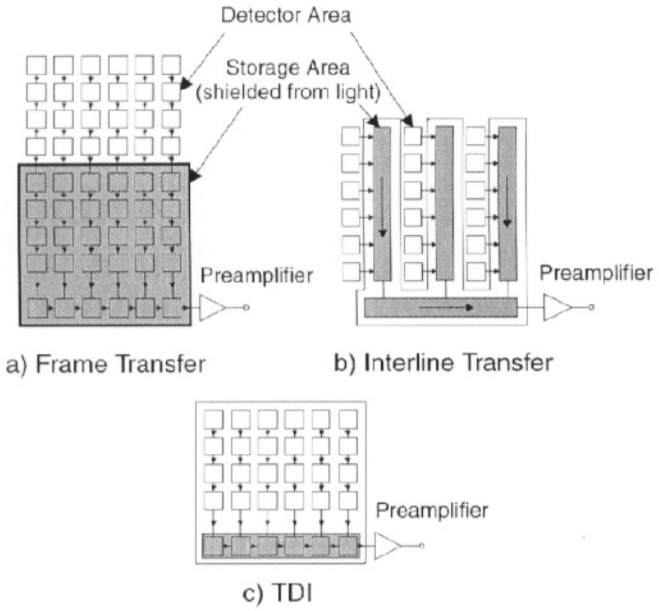

Figure 20. Typical readout configurations of CCDs showing (*a*) the frame transfer, (*b*) interline transfer and (*c*) time delay integration (TDI) devices. In (*a*) and (*b*) readout storage areas which are shielded from illumination are required.

over 100 transfers and 37% over 1000 transfers. The effect of less-than-perfect transfer efficiency is smearing of the image in the readout direction. In commercial CCDs, values of ε as high as 0.999999 are achievable.

Also of importance is the well storage capacity of the device. Depending on pixel size, capacities of 300 000 to several million electrons are possible. CCDs designed for video applications tend to be designed to have extremely small (15 μm) pixel dimensions. For medical applications, a larger size (25–100 μm) is generally desirable because this offers greater well capacity and better conforms with other constraints on spatial resolution.

It is important that the CCD be designed with appropriate 'anti-blooming' protection to prevent degradation of the image if some of the charge wells are overfilled. This can occur in situations where the x-ray detector is exposed to the unattenuated x-ray beam, for example at the edges of the patient. When the CCD is used in TDI mode, the well capacity must be such that the integral charge over all stages of integration can be accommodated. For example, if each detector element accumulates 50 000 electrons per row and there are 64 rows in the CCD over which integration will take place, the well capacity must be 3.2 million electrons.

9. Possible replacements for the XRII

Digital systems based on the use of XRIIs have several disadvantages: the bulky nature of the intensifier, which often impedes the clinician by limiting access to the patient and prevents the acquisition of some important radiographic views; loss of image contrast due to x-ray and light scatter within the tube i.e. veiling glare; geometric (pincushion) distortion of the image also largely due to the curved input phosphor and 'S' distortion which is

attributable to the earth's magnetic field.

While it is very easy to find fault with the XRII, its longevity points to the fact that it must be doing most things well. Perhaps its most important feature is that it is x-ray quantum limited over a huge range of input exposure levels. This is possible because it is an electrostatic imaging device. To couple the image to the next stage efficiently, it is important that the image be reduced from the large format at the input to the XRII. In comparing the electrostatic and optical format reduction as shown in figure 12, it can be seen that in the optical situation much of the light emitted from the screen is lost and the proportion of light lost increases rapidly as the demagnification factor is increased (see also figure 13). In an electrostatic system such as the XRII, the light from the phosphor is efficiently coupled to the photocathode and the emitted electrons are efficiently collected and accelerated to provide amplification. This avoids a secondary quantum sink, often a problem with optical coupling.

9.1. X-icon system

An alternative approach which eliminates the need for the conventional XRII is the X-icon. This is a directly x-ray sensitive, large-area video camera. In principle, the whole fluoroscopic imaging chain (XRII, optical distributor and multiple optical devices) could be replaced by a large-area X-icon whose signal is distributed electronically and this goal has been pursued by several investigators (Keller and Ploke 1955, Nishida and Okamoto 1968, Jacobs 1980). Luhta and Rowlands (1993) have reviewed the history of X-icon development and described their progress toward this goal. Their system, illustrated in figure 21, is a single-stage device housed within a Pyrex glass vacuum vessel and containing a flat layer of approximately 500 μm thick amorphous selenium as the x-ray transducer. Otherwise, its operation is identical to that of the optical video camera described earlier. Due to the reduced number of stages compared with an XRII/video system it has the potential for higher resolution. It is inherently a flat-field device and thus problems of distortion and shading should be of a much less serious nature than for an XRII. X-ray sensitive vidicons have been investigated previously but none satisfied all the necessary requirements for medical application. Even if the technical features were adequate, an X-icon could not have been successful in the past because there was no useful system for (i) storing sequences of images created by video to replace the ciné camera or (ii) storing single high-quality small-format radiographs equivalent to those produced by the 100 mm photofluorographic camera. However, this gap has been bridged by the current availability of high-resolution video tape and disc recorders and digital frame stores.

10. Flat-panel systems

A flat-panel digital detector, in principle, could perform all current radiological modalities—radiography, fluoroscopy and fluorography. It could provide high image quality and an instant readout. Existing x-ray equipment could be easily adapted to employ such detectors. The technology of large-area active matrix arrays which would form the readout structure for a flat-panel system has been developed for liquid crystal displays (LCD) for over a decade.

Active matrix LCDs (AMLCDs) have been made using amorphous (hydrogenated amorphous silicon (*a*-Si:H) (Piper *et al* 1986, Powell 1989), polycrystalline (poly-Si) or cadmium selenide (CdSe) semiconductors (Brody *et al* 1984). During recent years, several manufacturers in Japan, Europe and North America have invested heavily in this

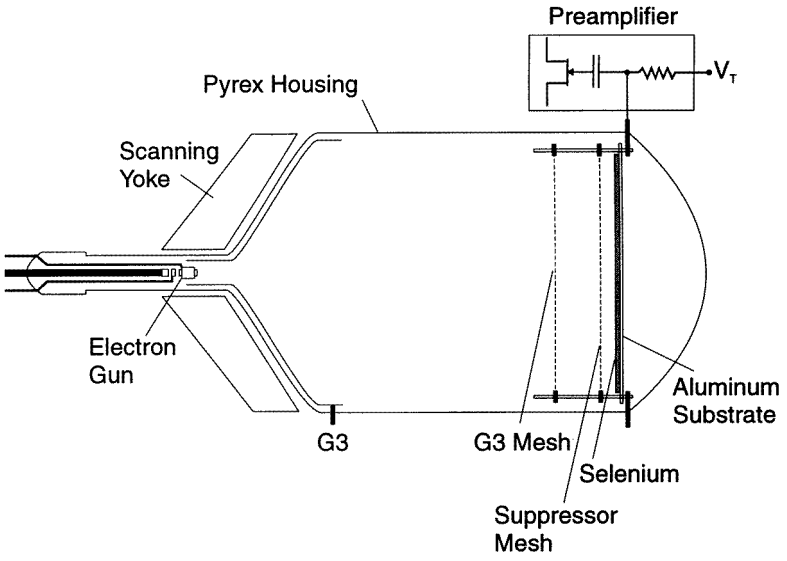

Figure 21. Direct conversion selenium vacuum tube imager (X-icon) capable of both radiographic and fluoroscopic operation. The evacuated Pyrex housing encloses the target of amorphous selenium deposited on an aluminium substrate. Electrons emitted by the gun are deflected by the scanning yoke and impinge on the target. Focus is established with the aid of the two-part G3 electrode. The supressor mesh is necessary to prevent loss of image stability under high illumination. This instability is due to the large target potential V_T required by the thick amorphous selenium layer. The signal is obtained directly from the target current and fed to the pre-amplifier.

development and it is becoming the preferred technology for lap-top computer displays. Each display panel consists of two sheets of glass with a uniform layer of liquid crystal in between. One sheet is the active matrix itself (i.e. a large-area integrated circuit consisting of a large number of thin film field-effect transistors (TFTs) connected to individual pixel electrodes in a matrix). The other sheet has a uniform electrode layer.

Two general approaches for flat-panel digital x-ray detectors are currently under investigation. In the first a phosphor layer is used to absorb x-rays and the resultant light photons are detected by a large-area photodiode array read out with active devices (for example, thin film transistors or diode switches) integrated onto the plate at each pixel (Antonuk *et al* 1991, Fujieda *et al* 1993). In the second approach (sometimes called the direct method), x-rays are detected in an amorphous selenium layer and the resulting charges released are collected on individual pixel electrodes. Finally, the readout occurs using the active matrix as in the indirect method.

The potential advantages of such self-scanned, readout systems include their compactness permitting better access to patients than bulky devices such as conventional XRIIs. Since they are flat, they can be expected to be largely free from veiling glare, geometrically uniform. Unlike XRIIs they are immune to stray magnetic fields. These properties facilitate quantitative image analysis, registration and clinical comparison of images from other modalities, 3D reconstruction applications such as cone beam volume CT (Ning *et al* 1991), and use in magnetic environments such as MRI rooms.

10.1. Phosphor flat-panel detectors

Several groups are developing large-area photodetector arrays composed of individual photodiodes made with amorphous silicon, onto which a conventional x-ray absorbing phosphor, such as Gd_2O_2S, is placed or thallium-doped caesium iodide (CsI:Tl) is grown (Perez-Mendez *et al* 1989, Fujieda *et al* 1991).

The principle of operation of an amorphous silicon detector is shown schematically in figure 22. The detector pixels are configured as photodiodes (figure 22(*a*)) which convert the optical signal from the phosphor to charge and store that charge on the pixel capacitance. Being low-noise devices, the photodiodes provide a very large dynamic range, of the order of 40 000. A typical thin film transistor readout array is shown in figure 22(*b*). The signal is read out by activation of scanning control lines for each row of the device, connected to the gates of TFTs located on each detector pixel. An entire row of the detector array is activated simultaneously and the signal is read on lines for each column in the array which connects all the TFT sources in that column to a low-noise charge amplifier. The amplified signals from the columns are then multiplexed and digitized. This allows fast detector readout and requires a number of electronic channels equal to the number of columns of the array. Both radiographic (Antonuk *et al* 1992) and fluoroscopic (Schiebel *et al* 1994) systems have been described.

Alternatively, instead of TFT readout various diode switching schemes can be used (Chabbal *et al* 1996, Graeve *et al* 1996). The advantage of the diode approach is that since the photodiode has to be made anyway, the switching diode can be made at the same time without increase in the number of processing steps. The disadvantages of diode readout are a strong nonlinearity and large charge injection.

The area allocated to each pixel of the array must contain the photodiode, switching device and control and signal lines so that the fill factor is less than 100%. This potential loss of x-ray utilization efficiency becomes proportionately greater as the pixel size is decreased and provides a challenge for the application of this technology to very high-resolution applications.

The advantage of utilizing CsI as the x-ray absorber is that it can be grown in columnar crystals which act as fibre optics (figure 7(*b*)). When coupled to the photodiode pixels, there is little lateral spread of light and, therefore, high spatial resolution can be maintained. In addition, unlike conventional phosphors in which diffusion of light and loss of resolution become worse when the thickness is increased, CsI phosphors can be made thick enough to ensure a high value of η while maintaining high spatial resolution.

10.2. Solid state electrostatic systems

There are several advantages in the use of solid state electrostatic systems such as the photoconductor, amorphous selenium (a-Se), or the semiconductor, silicon, in high-purity, single-crystal form rather than phosphors. The basis of most medical x-ray imaging systems is a phosphor layer or 'screen' shown in figure 7(*a*). As discussed earlier, x-rays absorbed in the screen release light which must escape to the surface to create an image and lateral spread of light is determined by diffusion. Thus the blur diameter is comparable to the screen thickness. This blurring causes a loss of high-frequency image information which is fundamental (Sandrik and Wagner 1982) and largely irreversible. The loss can be alleviated by using a phosphor such as CsI which can be grown in the form reminiscent of a fibre optic (figure 7(*b*)). However, the separation between fibres is created by cracking and as a result the channelling of light is not perfect (Spekowius *et al* 1995). An alternative and possibly

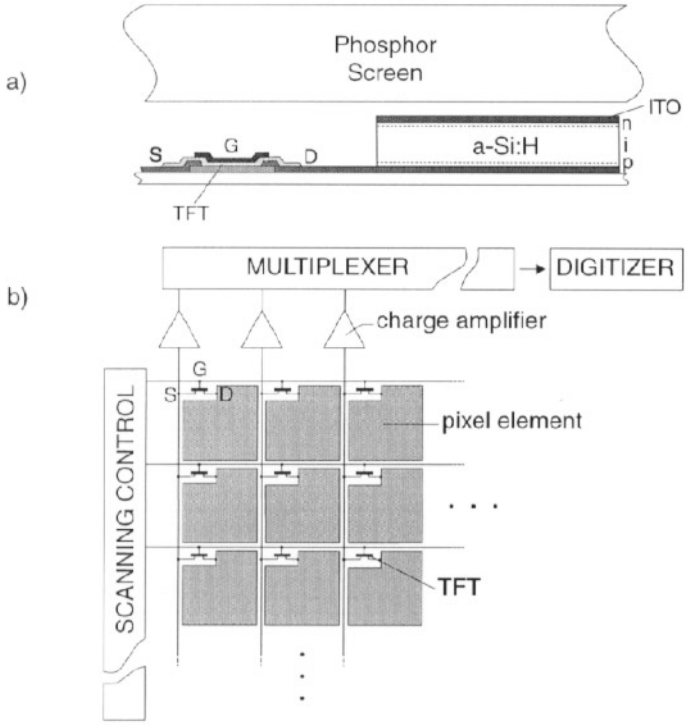

Figure 22. (*a*) Principle of amorphous silicon detector (cross-sectional view) showing thin film transistor (TFT) and the n-i-p a-Si:H photodiode with a transparent conductive indium tin oxide (ITO) electrode connected to a common bias of ~ 5 V. The other electrode of the photodiode is connected to the drain (D) of the TFT which acts as a switch, controlled by the potential on the gate (G), to connect the photodiode to the source (S). (*b*) Amorphous silicon matrix readout array of pixel elements (photodiodes) and thin film transistor switches which can be used to create a large-area detector. The scanning contol addresses the array line by line and the charge signals are read out along columns of the device connected to charge amplifiers.

preferable method is to use a structureless electrostatic layer (Brodie and Gutcheck 1982) as shown in figure 7(*c*). X-rays interacting in the photoconductor plate release electrons and holes, which, because they are charged, can be guided directly to the surfaces of the photoconductor by the applied electric field. The latent charge image on the photoconductor surface is, therefore, not blurred significantly even if the plate is made thick enough to absorb most incident x-rays (Que and Rowlands 1995).

Amorphous selenium (a-Se) is the most highly developed photoconductor for x-ray applications. Its amorphous state makes possible the maintenance of uniform imaging characteristics to almost atomic scale (there are no grain boundaries) over large areas. The primary function of the a-Se layer is to attenuate x-rays, generate free electron–hole pairs (in proportion to the intensity of the incident x-rays) and collect them at the electrodes. To achieve a high value of η, the detector must be of adequate thickness (figure 4). High efficiency in converting absorbed x-ray energy into free electron–hole pairs requires high electric fields. Finally, the number of bulk traps in the layer must be small so that virtually all the freed carriers reach their appropriate electrode. Each surface must have an electrode attached to permit collection of charge from the a-Se while preventing entry of charge from

the electrodes into the a-Se. This is called a *blocking contact*, which must be maintained even under very high electric fields (Schaffert 1980). Finally the surface of the a-Se at which the image is formed must have a very small transverse conductivity, otherwise the image charge could migrate laterally and destroy the resolution. The small transverse conductivity is achieved by introducing a high density of traps in the a-Se very close to the image interface. (Pai and Springett 1993).

The first medical application of a-Se, xeroradiography (Boag 1973)—where a latent charge image on the surface of an a-Se plate was read out with toner—was a technical and commercial success in its day. Though xeroradiography (see Jeromin 1988) is no longer competitive, this is probably more because of the toner readout method used at that time, rather than the underlying properties of a-Se (Brodie and Gutcheck 1985). Thus, by employing an electronic readout, a-Se again becomes feasible as the basis of a clinical imaging system.

Neitzel *et al* (1994) described a commercially available a-Se drum scanner for chest radiography. This is similar to earlier work by Xerox (Jeromin and Klynn 1979) and Philips at their Research Laboratories in Aachen (Hillen *et al* 1988) in which readout is accomplished by scanning a linear array of tiny electrometers over the electrostatic image on the selenium surface. May and Lubinski (1993) described a method to read out an a-Se plate with a phosphor-coated toner and laser scanner. They showed highly detailed images which were thought to be suitable for mammography. Cook *et al* (1994) have published preliminary descriptions of their recent work on laser discharge readout of a-Se. This work is related to much earlier publications by Korn *et al* (1978), Zermeno *et al* (1979), and DeMonts and Beaumont (1989) as well as the air-gap readout method (Rowlands *et al* 1991) and readout with a condensed state dielectric (Rowlands and Hunter 1995).

Lee *et al* (1996) have described a flat-panel method for radiography, based on the use of an active matrix readout method for a-Se and a similar approach has also been advocated by Zhao and Rowlands (1992, 1995) for radiography and fluoroscopy. The potential features of this method are: high image quality, real-time readout rate and compact size. The basic concept is shown in figure 23. During x-ray exposure, energy is absorbed by the a-Se layer and the charge created is drawn by the internal electric field E_{Se} to the surfaces. The image charge is collected by the pixel electrode and accumulated onto the pixel capacitance (i.e. self-capacitance and an integrated storage capacitor). The pixel electrode and storage capacitor are connected to the TFT switch of each pixel. The readout device can be similar to that used with amorphous silicon (figure 22(*b*)). The external scanning control circuit generates pulses to turn on all the TFT switches on a row of the array and transfers charge from the pixel capacitors to the readout rails (columns). The charge is then collected and amplified by an amplifier on each rail and the data for the entire row are multiplexed out. (The amplifiers and multiplexer are in another single-crystal silicon integrated circuit which is wirebonded to the array.) This sequence is repeated for each row of the array. The readout can be in real-time thus this approach has the potential to be used both in radiography and fluoroscopy. Fahrig *et al* (1995) have analysed the factors influencing DQE in a-Se x-ray detectors.

11. Other direct conversion systems

The advantages of direct conversion of the x-ray signal to electric charge are obvious. Problems associated with secondary quantum sinks are eliminated and bulky optical coupling elements are not required. One material which can be used for direct conversion is crystalline silicon. Silicon has been used for x- and gamma-ray spectroscopy as well as dosimetry. A

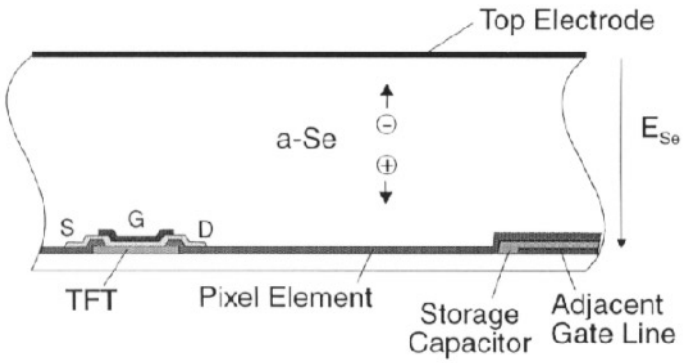

Figure 23. Principle of amorphous selenium area detector (see also figure 22(*b*) for the readout configuration). The a-Se layer is evaporated directly onto an active matrix array in which the pixel elements are simply electrodes. An electric field E_{Se} is established across the selenium by applying an appropriate high voltage to the common top electrode on the a-Se layer. The charge released by radiation is collected by the electric field on a capacitor made, for example, by overlapping the pixel electrode and an adjacent gate line.

simple P-I-N photodiode construction can also be configured as an x-ray imaging detector. Silicon produces an electron–hole pair for each 3.6 eV deposited in the crystal (table 1), so a 40 keV quantum will produce 11 100 electron–hole pairs. These can be efficiently collected from the depleted region of the diode by an electric field placed across this region. Such a detector can be operated at room temperature, but the thermal noise characteristics can be improved considerably by cooling to a few degrees celsius. The photodiodes can be produced with very fine pitch, essentially limited only by the number of quanta that are to be collected in a pixel, i.e. by the acceptable noise level and patient dose.

As seen in figure 4, silicon, because of its low Z and density, is not an efficient x-ray absorber at higher energies, and to achieve an acceptable value of η, even at mammographic energies, the detector must be at least 1 mm thick. For high-resolution detectors ($p = 50$ μm), this implies that quanta striking the detector entrance surface at some distance from the central ray of the x-ray beam will, because of the non-normal incidence, be likely to be absorbed in an adjacent detector element, causing geometrical broadening of the line spread function. To avoid this problem, the detector array can be arranged along a curved surface, with the radius of curvature equal to the source image plane distance (SID) as shown in figure 24(*a*). One method of producing this type of detector (figure 24(*b*)) is as a hybrid between a pixellated array of photodiodes and a TDI CCD readout formed on a separate substrate. The two matrices are joined on a pixel-by-pixel basis by a series of microscopic indium 'bumps'. Thus charge liberated in the photodiodes is collected and integrated down CCD columns and finally digitized. Detectors of this design were initially used for imaging in the infrared spectrum and have been shown to provide very high spatial resolution and other desirable imaging characteristics when modified for use with x-rays (Henry *et al* 1995). It is likely that in the future, more x-ray absorbent detector materials for the photodiodes such as zinc cadmium telluride, mercuric iodide or thallium bromide (Shah *et al* 1989) will be available and will offer higher η for thinner detector structures making such direct conversion detectors much more practical.

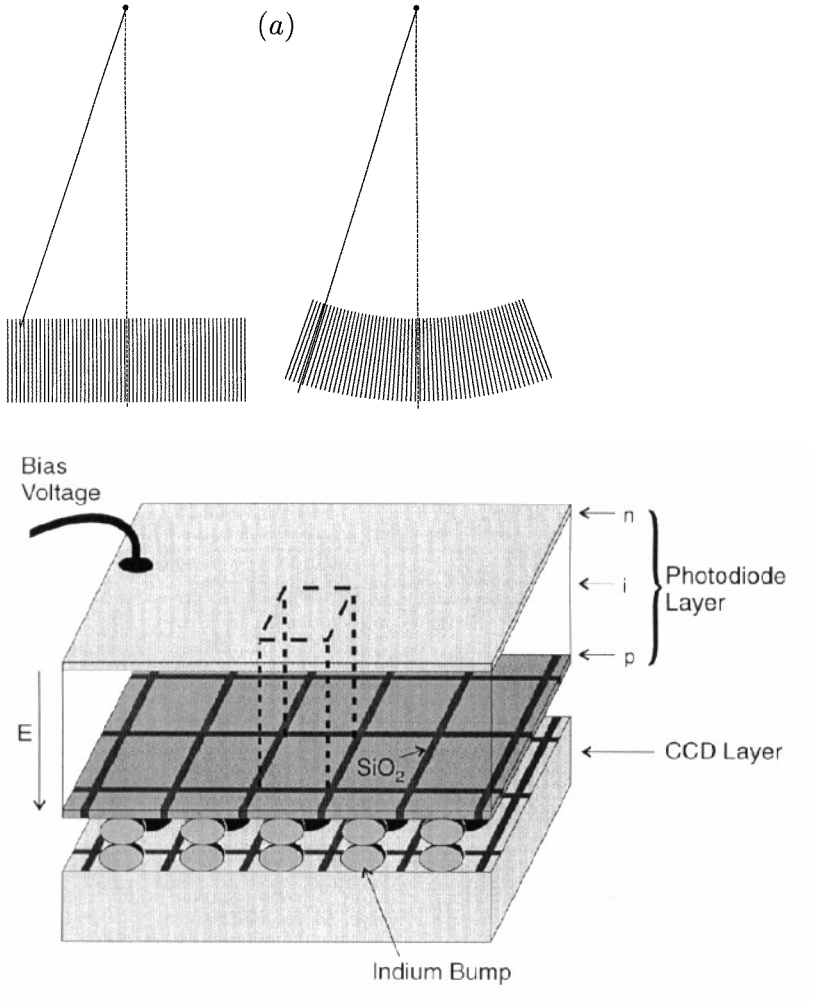

(*b*)

Figure 24. (*a*) Detectors employing low-Z, low-density materials must be thick to achieve reasonable values of η. To avoid loss of resolution due to geometric spread of signal the detectors must be curved so that the x-rays are at normal incidence. (*b*) A hybrid detector that can employ crystalline silicon or zinc cadmium telluride as the x-ray absorber. The detector pixels are each connected to elements of a CCD in the readout layer below.

12. Conclusion

There are a number of possible approaches for producing detectors for digital radiography, although there may not be a single technology that is optimal for all applications. The technology of choice will depend on spatial resolution and geometry requirements as well as the necessary imaging speed and acceptable cost. Optimization will require careful attention to the specification of the clinical imaging task and the key image information that is required of the examination. Close interaction with the radiologist and the clinician will help ensure that the imaging technology appropriately meets these requirements.

Acknowledgments

The authors gratefully acknowledge the financial support of their research on digital radiography by the National Cancer Institute of Canada through a Terry Fox Programme Project Grant entitled 'Medical Imaging for Cancer'.

References

Antonuk L E, Boudry J, Kim C W, Longo M J, Morton E J, Yorkston J and Street R A 1991 Signal, noise, and readout considerations in the development of amorphous silicon photodiode arrays for radiotherapy and diagnostic imaging *Proc. SPIE* **1443** 108–19

Antonuk L E, Boudry J, Wang W, McShan D, Morton E J, Yorkston J and Street R A 1992 Demonstration of megavoltage and diagnostic x-ray imaging with hydrogenated amorphous silicon arrays *Med. Phys.* **19** 1455–66

Arnold B and Scheibe P O 1984 Noise analysis of a digital radiography system. *Am. J. Radiol.* **142** 609–13

Baily N A 1980 Video techniques for x-ray imaging and data extraction from roentgenographic and fluoroscopic presentations *Med. Phys.* **7** 472–91

Barrett H and Swindell W 1981 *Radiological Imaging* (New York: Academic) pp 285–8

Bendat J S and Piersol A G 1986 *Random Data Analysis and Measurement Techniques* 2nd Edn (New York: Wiley) p 338

Boag J W 1973 Xeroradiography *Phys. Med. Biol.* **18** 3–37

Bogucki T M, Trauernicht D P and Kocher T E 1995 Characteristics of a storage phosphor system for medical imaging *Technical and Scientific Monograph* No 6 (Eastman Kodak Health Sciences Division)

Boyle W S and Smith G E 1970 Charge-coupled semiconductor devices *Bell Syst. Tech. J.* **49** 587

Brodie I and Gutcheck R A 1982 Radiographic information theory and application to mammography *Med. Phys.* **9** 79–95

——1985 Minimum exposure estimates for information recording in diagnostic radiology *Med. Phys.* **12** 362–7

Brody P, Luo F C and Malmbert P 1984 Active-matrix addressing enhances flat panels *Electronics* July 12 113–7

Bunch P C, Huff K E and Van Metter R 1987 Analysis of the detective quantum efficiency of a radiographic screen-film combination *J. Opt. Soc. Am.* A **4** 902–9

Chabbal J *et al* 1996 Amorphous silicon x-ray sensor *Proc SPIE* **2708** 499–510

Chan H P, Doi K, Galhotra S, Vborny C J, MacMahon H and Jokich P M 1987 Image feature analysis and computer-aided diagnosis in digital radiography. 1. Automated detection of microcalcifications in mammography *Med. Phys.* **14** 538–48

Cook E L, Edwards J D, Nelson O L and Potts J E 1994 Performance of a high resolution radiographic detector *The Society of Imaging Science and Technology 47th Ann. Conf. and Int. Committee on the Science of Photography, ICPS'94* (Springfield, VA: IS&T) Extended Abstracts pp 699

Cunningham I A, Westmore M S and Fenster A 1994 A spatial frequency dependent quantum accounting diagram and detective quantum efficiency model of signal and noise propagation in cascaded imaging systems *Med. Phys.* **21** 417–27

DeGroot P M 1994 Image intensifier design and specifications *Proc. Summer School on Specification, Acceptance Testing and Quality Control of Diagnostic X-ray Imaging Equipment* ed J A Seibert, G T Barnes and R G Gould (Woodbury, NY: AIP) pp 429–60

DeMonts H and Beaumont F 1989 A new photoconductor imaging system for digital radiography *Med. Phys.* **16** 105–9

DiBianca F A and Barker M D 1985 Kinestatic charge detection *Med. Phys.* **12** 339–43

Dobbins J T III 1995 Effects of undersampling on the proper interpretation of modulation transfer function, noise power spectra, and noise equivalent quanta of digital imaging systems *Med. Phys* **22** 171–81

Drangova M and Rowlands J A 1986 Optical factors affecting the detective quantum efficiency of radiographic screens *Med. Phys.* **13** 150–7

Evans R D 1955 *The Atomic Nucleus* (New York: McGraw-Hill)

Fahrig R, Rowlands J A and Yaffe M J 1995 X-ray imaging with amorphous selenium: Detective quantum efficiency of photoconductive receptors for digital mammography *Med. Phys.* **22** 153–60

Feig S A and Yaffe M J Digital mammography, computer-aided diagnosis, and telemammography *Radiol. Clin. N. Am.* **33** 1205–30

Fraser R G *et al* 1989 Digital imaging of the chest *Radiology* **171** 297–307

Fujieda I, Cho G, Drewery J, Gee T, Jing T, Kaplan S N, Perez-Mendez V and Wildermuth D 1991 X-ray and charged particle detection with CsI(Tl) layer coupled to a-Si:H photodiode layers *IEEE Trans. Nucl. Sci.* **38** 255–62

Fujieda I, Street R A, Weisfield R L, Nelson S, Nylen P, Perez-Mendez V and Cho G 1993 High sensitivity readout of 2D a- Si image sensors *Japan. J. Appl. Phys.* **32** 198–204

Giger M L, Ahn N, Doi K, MacMahon H and Metz C E 1990 Computerized detection of pulmonary nodules in digital chest images: use of morphological filters in reducing false-positive detections *Med. Phys.* **17** 861–5

Goodman L R, Wilson C R and Foley W D 1988 Digital imaging of the chest: promises and problems *Am. J. Radiol.* **150** 1241–51

Graeve T, Li S, Alexander S M and Huang W 1996 High-resolution amorphous silicon image sensor *Proc SPIE* **2708** 494–8

Hejazi S and Trauernicht D P 1996 Potential image quality in scintillator CCD-based imaging systems for digital radiography and digital mammography *Proc. SPIE* **2708** 440–9

Henry J M, Yaffe M J, Pi B, Venzon J E, Augustine F and Tumer T O 1995 Solid state x-ray detectors for digital mammography *Proc. SPIE* **2432** 392–401

Hillen W, Schiebel U and Zaengel T 1987 Imaging performance of a digital storage phosphor system *Med. Phys.* **14** 745–51

——1988 A selenium-based detector system for digital slot-radiography *Proc. SPIE* **914** 253–61

Hounsfield G N 1973 Computerized transverse axial scanning (tomography): Part I *Br. J. Radiol.* **46** 1016–22

Hynes D M, Rowlands J A and Edmonds E W 1989 Clinical comparison of analog and digital 100 mm photofluorography *J. Can. Assoc. Radiol.* **40** 262–5

Jacobs J E 1980 X-ray sensitive television camera tubes *Real-time Radiological Imaging: Medical and Industrial Applications* (Philadelphia, PA: ATSM) p 90

Jeromin L S 1988 Electroradiography *Encyclopedia of Medical Devices and Instrumentation* vol 2, ed J G Webster (New York: Wiley) pp 1146–68

Jeromin L S and Klynn L M 1979 Electronic recording of x-ray images *J. Appl. Photo. Eng.* **5** 183–9

Karellas A, Harris L J, Liu H, Davis M A and D'Orsi C J 1992 Charge-coupled device detector: performance considerations and potential for small-field mammographic imaging applications *Med. Phys.* **19** 1015–23

Kasap S O 1991 Photoreceptors: the selenium alloys *Handbook of Imaging Materials* ed A S Diamond (New York: Marcel Dekker) pp 329–77

Kato K 1994 Photostimulable phosphor radiography design considerations *Specification, Acceptance Testing and Quality Control of Diagnostic X-ray Imaging Equipment* ed J A Seibert, G T Barnes and R G Gould (American Association of Physicists in Medicine Monograph #20) (Woodbury, NY: AIP) pp 731–69

Keller M and Ploke M 1955 Visual displays of x-ray photographs using a television camera tube which responds to x-rays *Z. Angew. Phys.* **7** 562–71 (In German. Translation available: Document 08Q70G- 1162-GJ Associated Technical Services, Inc., Glen Ridge, NJ, USA)

Klein C A 1968 Bandgap dependence and related features of radiation ionization energies in semiconductors *J. Appl. Phys.* **39** 2029

Korn D M, Johnson S P, Nelson O L and Ziegler R J 1978 A method of electronic readout of electrophotographic and electroradiographic images *J. Appl. Photogr. Eng.* **4** 178–82

Lee D L Y, Cheung L K, Palecki E F and Jeromin L S 1996 A discussion on resolution, sensitivity, S/N ratio and dynamic range of Se-TFT direct digital radiographic detector *Proc. SPIE* **2708** 511–22

Luhta R and Rowlands J A 1993 X-ray sensitive video camera *Proc. SPIE* **1896** 38–49

Maidment A D A, Fahrig R and Yaffe M J 1993 Dynamic range requirements of x-ray detectors for digital mammography *Med. Phys.* **20** 1621–33 (see also letter in *Med. Phys.* **21** 1215)

Maidment A D A and Yaffe M J 1994 Analysis of the spatial-frequency dependent DQE of optically coupled digital mammography detectors *Med. Phys.* **21** 721–9

——1996 Analysis of signal propagation in optically coupled detectors for digital mammography: II lens and fibre optics *Phys. Med. Biol.* **41** 475–93

May J W and Lubinski A R 1993 High resolution computed radiography by scanned luminescent toner radiography *Proc. SPIE* **1896** 292–312

McGee J D 1979 The history of electronic imaging *Electronic Imaging* ed T P McLean and P Schagen (London: Academic) pp 11–54

McGinty G P 1984 *Video Cameras: Operation and Servicing* (Indianapolis: Howard Sams)

Miller L D 1971 Transfer characteristics and spectral response of television camera tubes *Photoelectronic Imaging Devices* vol 1, ed L M Biberman and S Nudelman (New York: Plenum) pp 267–90

Munro P, Rawlinson J A and Fenster 1990 Digital fluoroscopic imaging device for radiotherapy localization *Int. J. Radiat. Oncol. Biol. Phys.* **18** 641–9

Neitzel U 1994 Discernable gray levels and digitization requirements in digital mammography *Med. Phys.* **21** 1213–4

Neitzel U, Maack I and Guenther-Kohlfahl S 1994 Image quality of a digital chest radiography system based on a selenium detector *Med. Phys.* **21** 509–16

Ning R, Barsotti J B and Kido D K 1991 Clinical image-intensifier-based volume CT imager for angiography, Medical Imaging V: Imaging Physics *Proc. SPIE* **1443** 236–49

Nishida R and Okamoto S 1968 An x-ray sensitive vidicon *J. Inst. TV Engr. Japan* **20** 192

Nishikawa R M, Mawdsley G E, Fenster A and Yaffe M J 1987 Scanned projection digital mammography *Med. Phys.* **14** 717–27

Pai D M and Springett B E 1993 The physics of electrophotography *Rev. Mod. Phys.* **65** 163–211

Perez-Mendez V, Cho G, Fujieda I, Kaplan S N, Qureshi S and Street R A 1989 The application of thick hydrogenated amorphous silicon layers to charged particle and x-ray detection *Mater. Res. Soc. Symp. Proc.* **149** 621–30 (also *Lawrence Berkeley Laboratories Report* LBL-26998 April 1989)

Piper W, Bigelow J E, Castleberry D E and Possin G E 1986 The demands on the a-Si FET as a pixel switch for liquid crystal displays *Proc. SPIE* **617** 10–5

Powell M 1989 The physics of amorphous-silicon thin-film transistors *IEEE Trans. Electron Devices* **36** 2753–63

Que W and Rowlands J A 1995 X-ray imaging using amorphous selenium: inherent resolution *Med. Phys.* **22** 365–74

Rabbani M, Shaw R and Van Metter R 1987 Detective quantum efficiency of imaging systems with amplifying and scattering mechanisms *J. Opt. Soc. Am.* A **4** 895–901

Roehrig H, Fajardo L Yu T and Schempp W V 1994 Signal, noise and detective quantum efficiency in CCD-based x-ray imaging systems for use in mammography *Proc. SPIE* **2163** 320–32

Rose A 1948 The sensitivity performance of the eye on an absolute scale *J. Opt. Soc. Am.* **38** 196

Rougeot H 1993 Direct x-ray photoconversion processes *Digital Imaging: AAPM 1993 Summer School Proc.* ed W Hendee and J Trueblood (AAPM Monograph 22) (Madison, WI: Medical Physics Publishing) pp 49–96

Rowlands J A 1994 Fluoroscopic systems and viewing considerations *Proc. Summer School on Specification, Acceptance Testing and Quality Control of Diagnostic X-ray Imaging Equipment* ed J A Seibert, G T Barnes and R G Gould (Woodbury, NY: AIP) pp 483–98

Rowlands J A and Hunter D M 1995, X-ray imaging using amorphous selenium: Generalised analysis of Photo-induced discharge (PID) readout methods *Med. Phys.* **22** 1983–96

Rowlands J A, Hunter D M and Araj N 1991 X-ray imaging using amorphous selenium: A photoinduced readout method for digital mammography *Med. Phys.* **18** 421–31

Rowlands J A, Hynes D M and Edmonds E W 1989 System for digital acquisition of gastrointestinal images *Med. Phys.* **16** 553–60

Sanada S, Doi K, Xu X-W, Yin F-F, Giger M L and MacMahon H 1991 Comparison of imaging properties of a computed radiographic system and screen-film systems *Med. Phys.* **18** 414–20

Sandrik J M and Wagner R F 1982 Absolute measures of physical image quality: measurement and application to radiographic magnification *Med. Phys.* **9** 540

Schaffert R M 1980 *Electrophotography* (London: Focal) p 284

Schiebel U W, Conrads N, Jung N, Weilbrecht M, Wieczorek H, Zaengel T, Powell M J, French I D and Glasse C 1994 Fluoroscopic x-ray imaging with amorphous silicon thin-film arrays *Proc. SPIE* **2163** 129–40

Shah K S, Lund J C, Olschner F, Moy L and Squillante M R 1989 Thallium bromide radiation detectors *IEEE Trans. Nucl. Sci.* **36** 199–202

Spekowius G, Boerner H, Eckenbach W and Quadfleig P 1995 Simulation of the imaging performance of x-ray image intensifier/TV camera chains *Proc. SPIE* **2432** 12–23

Swank R K 1973 Absorption and noise in x-ray phosphors *J. Appl. Phys.* **44** 4199–203

Takahashi K, Kohda K and Miyahara J 1984 Mechanism of photostimulated luminescence in BaFX : Eu^{2+} (X = Cl, Br) *J. Lumin.* **31 & 32** 266

Tesic M, Mattson R A, Barnes G B, Sones R A and Stickney J B 1983 Digital radiography of the chest: design features and considerations for a prototype unit *Radiology* **148** 259–63

Thompsett M F 1979 Video-signal generation *Electronic Imaging* ed T P McLean and P Schagen (London: Academic) pp 55–101

von Seggern H, Voigt T, Knupfer W and Lange G 1988 Physical model of photostimulated luminescence of x-ray irradiated BaFBr : Eu^{2+} *J. Appl. Phys.* **64** 1405–12

Vosburg K G, Swank R K and Houston J M 1977 X-ray image intensifiers *Adv. Electron. Electron Phys.* **43** 205–44

Wagenaar D J and Terwilliger R A 1995 Effects of induced charge in the kinestatic charge detector *Med. Phys.* **22** 27–34

Yaffe M J 1993 Direct digital mammography using a scanned-slot CCD imaging system *Med. Progr. Through Technol.* **19** 13–21

——1994 Digital Mammography *Syllabus of Categorical Course on Technical Aspects of Mammography* ed A Haus and M J Yaffe (Oak Brook, IL: Radiological Society of North America) pp 275–86

Yaffe M J and Nishikawa R M 1994 X-ray imaging concepts: noise, SNR and DQE *Specification, Acceptance Testing and Quality Control of Diagnostic X-ray Imaging Equipment* ed J A Seibert, G T Barnes and R G Gould (American Association of Physicists in Medicine Monograph #20) (Woodbury, NY: AIP) pp 109–44

Zermeno A, Kirby T, Cowart R, Marsh L, and Ong P 1979 Laser readout of electrostatic images *Proc. SPIE* **173** 81–7

Zhao W and Rowlands J A 1992 A large area solid-state detector for radiology using amorphous selenium *Proc. SPIE* **1651** 134–43

——1995 X-ray imaging using amorphous selenium: Feasibility of a flat panel self-scanned detector for digital radiology *Med. Phys.* **22** 1595–2604